We are IntechOpen, the world's leading publisher of Open Access books Built by scientists, for scientists

6,900
Open access books available

185,000
International authors and editors

200M
Downloads

154
Countries delivered to

Our authors are among the

TOP 1%
most cited scientists

12.2%
Contributors from top 500 universities

CLARIVATE ANALYTICS
BOOK CITATION INDEX
INDEXED

WEB OF SCIENCE™

Selection of our books indexed in the Book Citation Index
in Web of Science™ Core Collection (BKCI)

Interested in publishing with us?
Contact book.department@intechopen.com

Numbers displayed above are based on latest data collected.
For more information visit www.intechopen.com

Urban Wind Energy Evaluation with Urban Morphology

Biao Wang

Abstract

Urban wind development is gathering energy and passion these years and is good for sustainable cities. This chapter tries to evaluate wind energy potential with study of urban form in a block scale (500 m × 500 m). CFD method is used for wind flow simulation. CFD parameter settings were validated and evaluated with wind tunnel experiment. Simple building forms (1–3 buildings) were tested for exploring the impact of building form on wind potential. Space over roof is proved to be most effective and practical position for developing wind energy in the urban environment. Ideal urban forms were tested for evaluating the impact of one single morphological parameter on wind potential over roof. Real urban forms were then evaluated and compared in order to reveal the impact of different urban form parameter on wind potential. Urban form unit models are then considered to understand the impact of a certain urban form feature on wind potential. Finally, a block model in Beijing is given for urban wind evaluation case study, including wind potential evaluation of every building roof in the model, wind turbine position evaluation, and economical cost analysis.

Keywords: urban wind energy, wind environment, urban form, urban block, CFD simulation

1. Introduction

The twenty-first century is an era of harmonious development between man and nature. Renewable energy development, as a means to achieve sustainable social development, plays an active and important role in dealing with the pressing problems of climate change, air pollution, urban energy shortage, and so on. The development of wind energy has a long history, but the formal use of wind power to generate electricity did not begin until the end of the nineteenth century. At present, most wind turbines are installed in the suburbs or seashore. In these places, wind resources are relatively abundant and the space available for wind turbines is relatively large, so we can see some large-scale wind turbines in the open plain area of suburbs, on the top of mountains, and on the seashore. Some large areas are used for wind farms, with tens or hundreds of large and medium-sized wind turbines working together. The electricity generated is generally transmitted to dense and populated urban areas through high-voltage cables. However, in some windy areas where many wind turbines are installed, there may have the phenomenon of "abandoned wind," that is, the wind farm will close or stop some wind turbines in order to reduce operation loss. The abandoned percentage may raise to 30 in some

windy area in western China. The reason is that, as wind energy is unstable, sometimes there is too much wind energy electricity generated, which cannot be timely transported out for use and storage. Besides, the regional government energy management and coordination problems may also lead to the difficulty of wind power transportation.

Therefore, considering the huge investment in wind farms and high-voltage lines and towers, and the electricity loss during the long-distance transmission from suburban wind farms to urban areas, as well as the impact of wind farm construction on the ecological environment, people are considering urban wind power development in these recent 20 years. Generally speaking, the feasibility of urban wind power development can be summarized as follows: (1) Avoiding long-distance grid transmission, power generation can be used on site or stored separately (urban wind power is generally distributed, a small amount of electricity can be effectively stored, but a large number of it is difficult; (2) there are many tall buildings in the city, whose top or side is usually accompanied by strong wind; and (3) small or micro wind power systems have small investment and are suitable for decentralized use by the whole people. They are also conducive to the participation of residents in the production and use of green energy.

As shown in literature, there appears to have increasing papers and project on the development of wind power in urban areas. In 1998, the European Union project "Wind Energy for the Built Environment" (WEB) first carried out the research on installing small wind turbines in urban environment, and developed a prototype of integrated wind turbine technology (UWECS: Urban Wind Energy Conversion Systems) [1, 2]. In the UK in 2003 and 2004, there was a project called BUWTs (the feasibility of building mounted/integrated wind turbines), which investigates and analyses the wind power technology in the building environment and aims at reducing carbon dioxide emissions [3]. In 2007, another European Union project, Wind Energy Integration in the Urban Environment, investigated the installation of small wind turbines in different regions and analyzed the feasibility, technology of wind turbines, as well as administrative and legal constraints on urban wind turbines in three European countries (UK, France, and the Netherlands) [4–7]. In addition, in 2004, the Regional Environment and New Energy Agency (ARENE) in France conducted a general study on the technical, economic, and management constraints of urban wind power generation with 60 installed wind turbines [8].

There are a certain number of books and thesis issued on the domain of urban wind energy. Yu [9] reviewed the current situation and development of wind energy in Hong Kong. Turesson [10] assessed renewable energy, mainly solar, wind, and biogas, in three European cities (Grenoble, Delft, and Växjö) in 2020. The assessment method was simple, but not fairly adapted to reality, because it uses the parameters of giant wind turbines higher than 100 m, which seldom adapts to urban environment. Shi [11] analyzed the use and storage of wind energy around urban buildings. Zeng [12] conducted wind and photovoltaic research in four blocks of Jinan, China, and proposed practical guidelines for urban renewable energy development. Within a more technical framework, Whaley [13] focused on low-cost generators for small wind turbines. The book "Windmill Power for City People" [14] provides a historical perspective on the city's first wind power generation system. The book "Urban Wind Energy" outlines several aspects of urban wind power plants [2]. Another book with the same title, published by [15], provides detailed examples of Gavle, Sweden, and conducted wind tunnel tests with the Gavlerinken Arena model to install two small wind turbines on the roof.

There are also many articles on this topic. Kalmikov et al. [16] evaluated wind energy potential at an attitude of 20 m in the Massachusetts Institute of Technology

campus through field measurement data analysis and CFD simulation. Zhao et al. [17] gave a general introduction on the integration of wind power and architecture. Balduzzi et al. [18] studied the flux with oblique incidence in the built environment and designed a new H-Rotor Darrieus wind turbine that can adapt to this flux on the roof. Stathopoulos et al. [19] and Anup et al. [20] made general reviews on the urban wind energy development and small wind turbines in the built environment. Simoes and Estanqueiro [21] presented an urban digital terrain model for urban wind resource assessment in city scale by mapping urban fabric and surrounding terrain. Toja-Silva et al. [22] presented a review on technical computational fluid dynamics (CFD) aspects relevant for urban wind energy exploitation and the current state-of-the-art in building aerodynamics applied to this field.

Building form and urban form have impact on wind flow pattern and energy potential. Biao et al. [23] had done a parametric study of the effect of building layout on wind flow in an urban context. A parameter called wind network index was defined to evaluate the effect of road network on ventilation. Asfour [24] used CFD simulation to investigate airflow behavior around different configurations of residential blocks. Liu et al. [25] conducted CFD simulation with site measured data on the impact of surrounding buildings in different radius distance on wind flow around a studied building. The results showed that the impact is considerable due to the sheltering and channeling effect. Azizi and Javanmardi [26] studied the effects of urban block forms on the patterns of wind and natural ventilation and found that two factors with the most effect on wind pressure difference were urban block height and widths of adjunct roads.

This chapter is based on the feasibility of urban wind energy and describes how to evaluate the potential of urban wind power through urban morphology. The general presentation of urban wind evaluation method and urban form classification can be found in previous study [27]. For case study, some primary results on urban wind potential evaluation with impact of urban form are published [28].

2. Methodology

2.1 Indicators of wind energy evaluation

To evaluate the effect of wind accumulation, there is an indicator used frequently called wind speed augmentation factor [29–31]:

$$C_v = \frac{U}{U_0} \tag{1}$$

where U is the actual wind speed of the test point and U_0 is the wind speed of free wind (in the wind field without buildings) with the same height of the point. U_0 can be calculated directly with the following equation.

$$U_z = U_h \left(\frac{z}{h}\right)^\alpha \tag{2}$$

where U_z is the wind velocity of the height z, U_h is the reference wind speed of the meteorological observation point at the height of h, and α is a roughness coefficient of the ground. For a dense city environment, the typical value of α is between 0.25 and 0.4.

However, the power of wind turbine is a function of the cube of wind velocity, defined as the following:

$$P = \frac{1}{2} C_p \rho A U^3 \tag{3}$$

where C_p is the power coefficient, ρ is the air density, A is the swept surface by the turbine blades, and U is the instant wind velocity.

As the wind augmentation factor can only show the wind velocity augmentation effect, we are thinking to find an indicator to evaluate wind energy with the cube of wind velocity. Therefore, a simplified indicator M can be defined as plane wind potential to evaluate wind energy on a given surface A:

$$M = \sum_{i=1}^{n} \left(A_i \times U_i^3 \right) \tag{4}$$

where A_i is the area of the corresponding velocity magnitude U_i. As shown in **Figure 1a, b**, the three red rectangular planes over roof at different heights (Z = 3, 5, or 10 m from the roof). Each plane is divided into several sub-areas according to the velocity scale (**Figure 1(c)**). For a given surface, each sub-area is multiplied with its corresponding cubic average velocity and then the multiplications can be summed up into the value of M [32].

As the plane surface (A) does not correspond to the swept area by the turbine blades (S), the value of M does not mean the actual wind energy power, rather the wind potential within a surface where turbines can be placed to exploit the wind energy. Besides, as wind velocity varies much more on the vertical height than on horizontal planes, concerning the operation difficulty we generally adopt the horizontal planes to evaluate the wind energy over roof.

In the actual calculation, we found that there is an indicator called "area-weighted average" that can be directly calculated by the code FLUENT. User-defined function (UDF) is used to create a parameter by a cubic wind velocity and then the software can import the area-weighted average cubic velocity (can be named as $\left(U^3 \right)_m$). Thus, an equivalent indicator M' is defined as follows:

$$M' = \left(U^3 \right)_m \times A \tag{5}$$

where A represents the evaluation plane area. The comparison analysis results show that the equivalent indicator M' can be used as the practical alternative of the indicator M, as there has very little difference between the two [33].
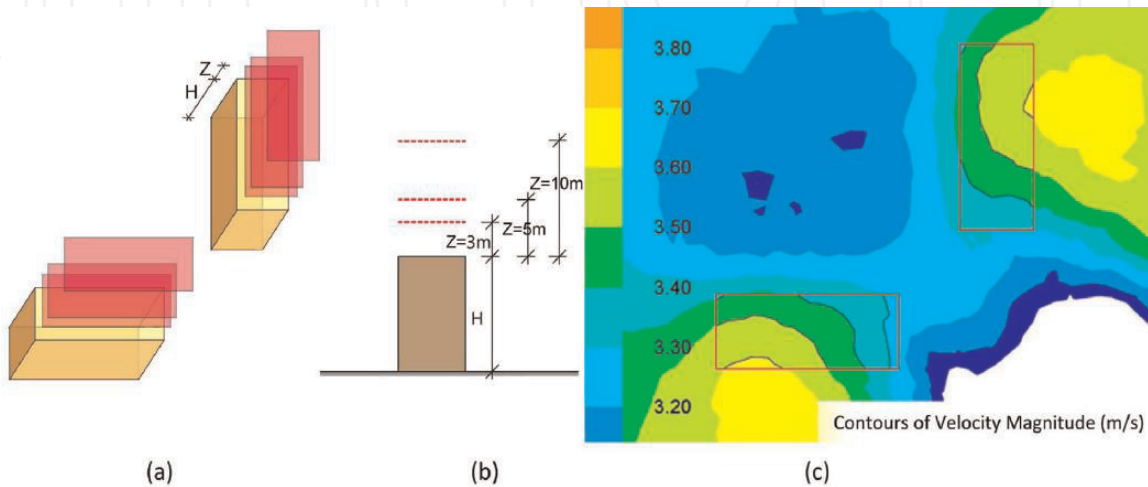
Figure 1.
Wind potential evaluation planes over roof of two perpendicular buildings: (a) perspective, (b) section, and (c) wind velocity contours [32].

Furthermore, to evaluate and compare wind potential on planes with different surface areas, we can define plane wind potential density as follows:

$$D = \left(U^3\right)_m = M/A \tag{6}$$

2.2 CFD setting and validation

When using CFD software to simulate wind flow in the built environment, there are a number of parameters needed to be regulated and validated in order to get a reasonable result. We adopted an open access database of wind tunnel experiment undergone by the Architectural Institute of Japan. A building of width 5 m × length 20 m × height 20 m was tested. For CFD simulation in the platform ANSYS 12.0, we took 57 tests in order to regulate different parameters of geometry, mesh, boundary condition, turbulence models, and solution method. The best choice setting found and the process of validation are shown in the article [32]. The results show a general good agreement between the CFD simulation and the experiment. The general average absolute error of the velocity magnitude is 0.37 m/s for an object velocity averaged 3.05 m/s in measurement.

When the simulation object turns from one or several buildings to a cluster of buildings, the scale is enlarged and the relationship between the group of building becoming important; therefore, the CFD setting need to be modified. Careful adjustments were taken for the case study of urban tissues with a dimension of around 500 × 500 m [27].

Apart from parameter validation by the tunnel experiment, there are some methods of verification that can be used: (1) Flow consistency analysis is to ensure the stability and credibility of CFD simulation results; (2) domain size analysis is to find a decent dimension of simulation domain in order to fully develop the turbulence and at the same time to avoid consuming much time for calculation; (3) grid sensibility analysis to ensure that the mesh size and method will not affect the results; and (4) random error analysis to assess the stability and sense of the findings during the CFD simulation process. The detailed methods explanation can be found in Ref. [33].
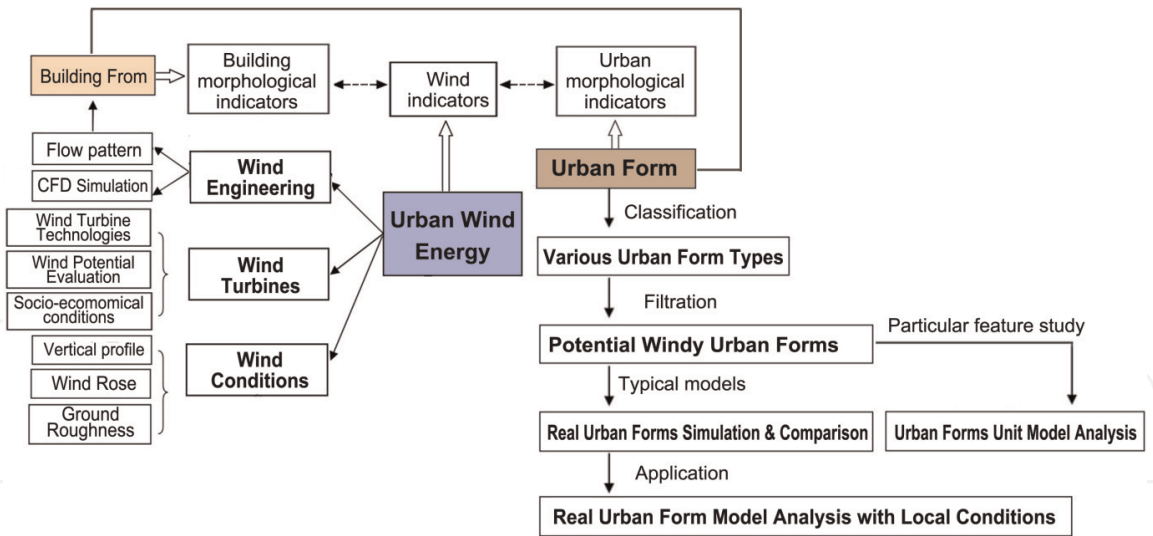
2.3 Research structure

There are two main domains for this research: urban form and wind potential. Two parts are integrated with cross indicator analysis and wind effect in the built environment. The detailed research structure is show in **Figure 2**.

For the part of urban wind energy, there are three related domains: wind engineering, wind turbines, and wind conditions. Wind flow pattern is influenced by the building forms. CFD simulation has its setting adapting to the nature of tested wind, and for the domain of wind flow simulation in the built environment, numerous experiments undergone by other scholars produced Best Practice Guideline for this domain [34, 35].

For the part of urban form study, first, from the global angle, different urban form types were classified; then with primary evaluation, some potential windy urban forms can be chosen. Some of the promising types would be used for CFD simulation and comparison, and some would also be used to extract single feature for close study through urban form unit model analysis. Case study of real urban form with local (environmental and socio-economical) conditions would be then analyzed for wind potential evaluation and urban wind development.

The relationship between urban wind energy and urban form can be evaluated by the correlation between wind energy indicators and urban morphological
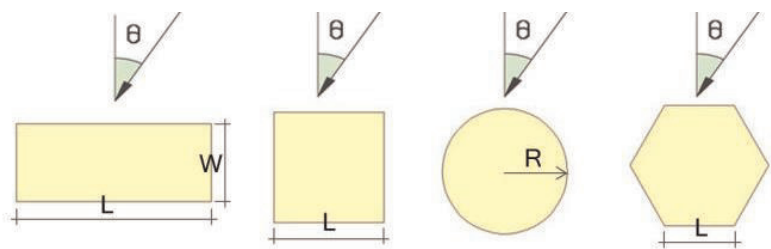
Figure 2.
Research structure.

indicators. As the building form is component and simple representation of urban form, the impact study of building form on wind is very beneficial to reveal the impact evaluation of urban form on wind. With its simplicity and less difficulty, the impact of different building morphological indicators on wind potential is analyzed before study the urban morphological indicators.

3. Building form and wind energy

3.1 Impact of building's floor plan on wind energy

In order to evaluate the influence of the building's floor plan on the wind potential above the roof, four models with the same height (H = 20 m) and the same floor plan area (S = 360 m^2) but different plane shapes (**Figure 3**) were tested. Concerning the symmetry aspect, only a range of 0–90° with increment of 15° for the inlet wind direction is considered; thus, each model has seven sessions of simulation.

Figure 4 shows the velocity profile of each model under normal wind with attitude z = 10 m. We can notice the difference in the size of the cyclones upstream and downstream, as well as the shape of the high-speed area around the building. However, what we are interested in here is comparing the wind power potential of all models. Through the simulation test, we noticed that the exploitable wind (with color of yellowish brown, red, or pink) near the plan generally has a relative long

Figure 3.
Models of buildings with different floor plans: Rectangular ($L \times W$ = 30 × 12 m), square (L = 19 m), round (R = 10.7 m), and hexagonal (L = 11.7 m).
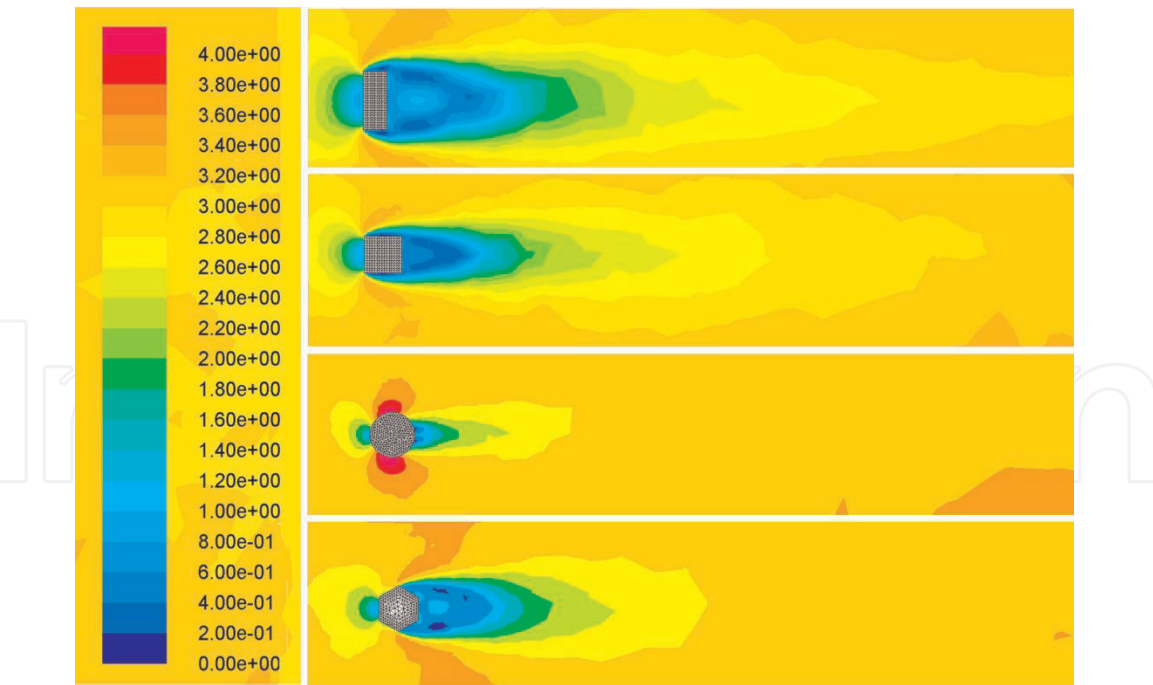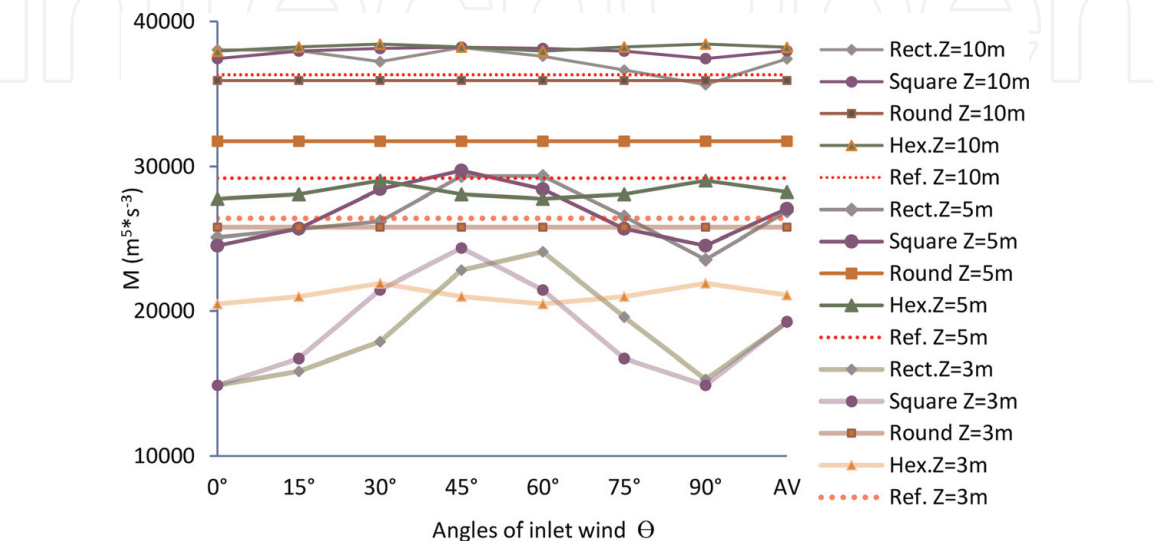
Figure 4.
Wind velocity profile around the buildings of different floor plans.

distance from the wall (except the model of round plan), so it is normally difficult to exploit this wind energy neither to fairly compare the models' exploitable wind potential. On the other hand, it is rather easy and accurate to evaluate the wind energy above the roof with the same plane surface for all the models studied.

Figure 5 shows the M values of the three heights above the roof (Z = 3, 5, 10 m). The following conclusions can be drawn:

1. On plane Z = 3 and 5 m, the M value on the roof of the round plan building is higher than that on the roofs of other buildings, but on plane Z = 10 m, it turns rather smaller than the others.

2. With the change of inlet wind angle, the M value over the roof of hexagonal buildings is almost monotonous. In fact, the gap between the best case (30°) and the worst (0°) of the three evaluation heights for this model is 1.28–6.55%.
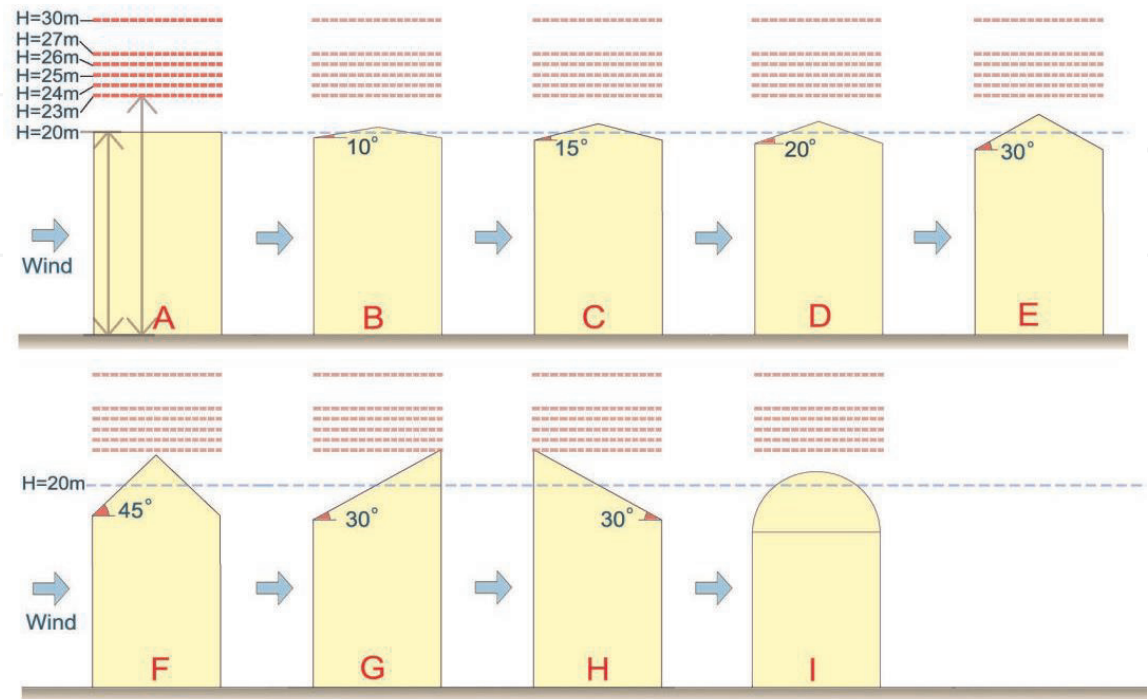

Figure 5.
Wind potential over roof of buildings with different floor plans.

3. The outcome of models with rectangular plan and square plan are very similar at a low altitude over roof (*Z* = 3 m). When the altitude rises to *Z* = 10 m, the square plan model becomes more attractive (more than 1.5%).

4. As far as the impact of inlet wind angle is concerned, an angle of 30° corresponds to the maximum wind potential over roof of the hexagonal plan model, while for rectangular plan model, it is 45° and for square plan model it is 60°.

5. At a low altitude above the roof, if no dominant wind is given, the wind energy density of different planes decreases with the following geometric shapes: round, hexagon, square, and rectangle. However, at high altitudes, the order changes: hexagon, square, rectangle, and round.

6. The wind potential of the free wind in the absence of buildings of the same height and the same initial conditions is marked as reference. We find that at *Z* = 3 m, *M* values of all models are lower than that of the reference, while at *Z* = 10 m, except for the round plan model, most models have higher values than the reference.

3.2 Impact of roof shape

In order to assess the effect of roof shape on the wind potential above the roof, nine buildings with the same plane (12 × 30 m) and equivalent height (*H* = 20 m) but different roof shapes were tested. The length (*L* = 30 m) of the buildings remains unchanged. Different roof shape models are considered here: A is reference model with flat roof, B, C, D, E and F are gable roof models with different roof gradients, G is wind-faced roof model, H is leeward roof model, and I is dome roof model (**Figure 6**). Due to the complexity of the flow over different shapes of roofs, we set six horizontal planes above the roof to evaluate wind flow over roof (see those discontinuous red lines in **Figure 6**). The heights from the ground of the planes are as follows: *H* = 23, 24, 25, 26, 27, and 30 m. In addition, due to the

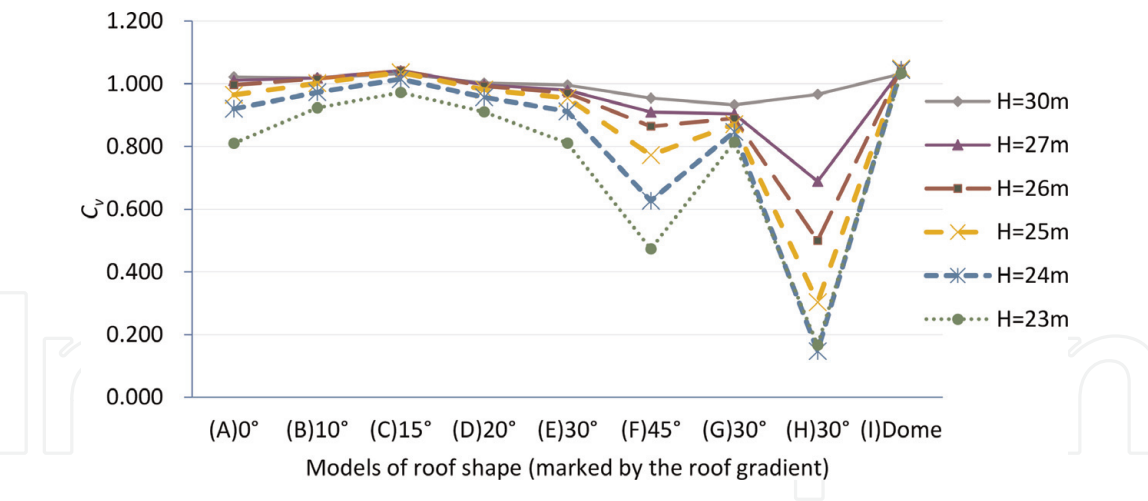**Figure 6.**
Different models of roof shapes (vertical section).

tremendous influence of turbulence in inclined wind, only wind with an incident angle of 0° is analyzed.

For this study, we use velocity augmentation coefficient Cv to assess the concentration of wind above the roof. Therefore, the average velocity values of six planes over roof are obtained directly from the flow, and the corresponding U_0 values are used to calculate the Cv values. From the results shown in **Figures 7** and **8**, we can find the following conclusions:

1. The average Cv values of the dome roof (model I) is the highest, and the height to reach the maximum Cv is $H = 25$ m.

2. In the gable roof group, the best way to collect wind energy is adopting roof with a slope of 15° (model C) at a capturing height of $H = 27$ m. In fact, at an altitude of $H > 24$ m, the coefficient of $Cv > 1$, i.e., for better utilization wind concentration effect, the evaluation altitude should be more than 24 m.

3. For the one-pitched roof, the wind-faced roof (model G) is generally more advantageous in wind concentration than the leeward roof (model H). However, it is still not as advantageous as the gable roof with the same gradient (model E).

In addition, in order to show the flow formation behind different roof shapes, the wind velocity variation in the central line in the wind direction at $H = 30$ m is presented (**Figures 9** and **10**). We have noticed that in the upstream of the buildings, the velocity difference among different models is very small, while in the downstream, the velocity difference is very large. For the gable roof models, the strongest wind behind the building is model C (a = 15°), followed by the model B
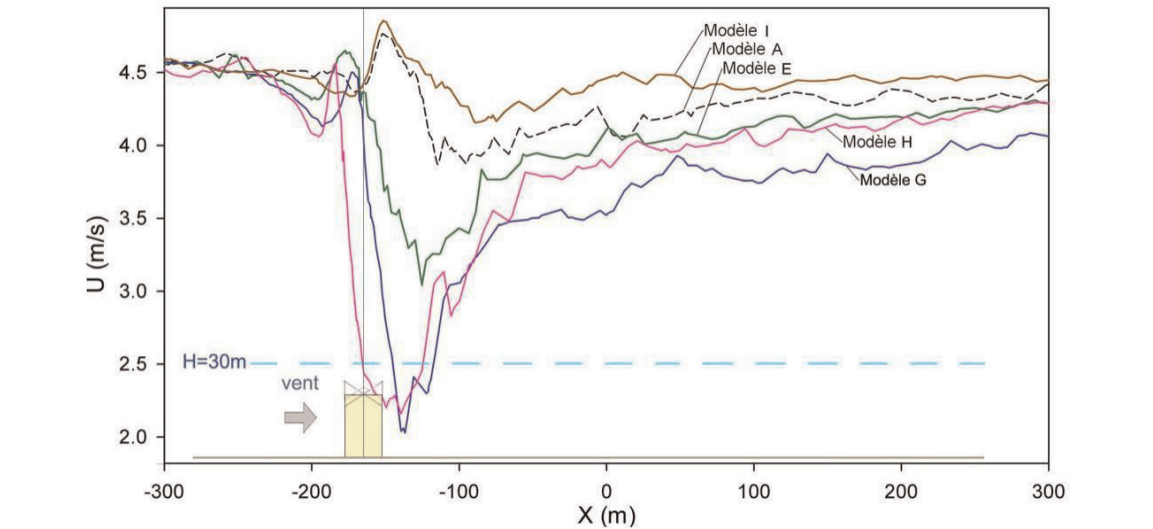

Figure 7.
Comparison of the coefficient Cv for different roof models.
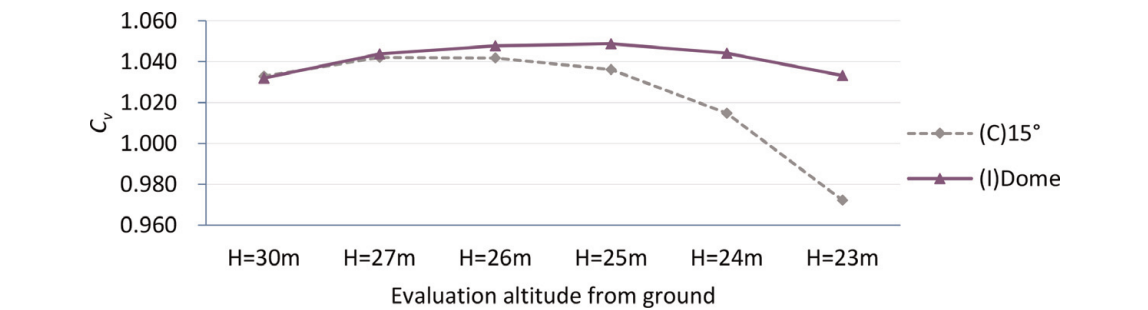
Figure 8.
Comparison of the coefficient Cv for roof models with different evaluation heights.
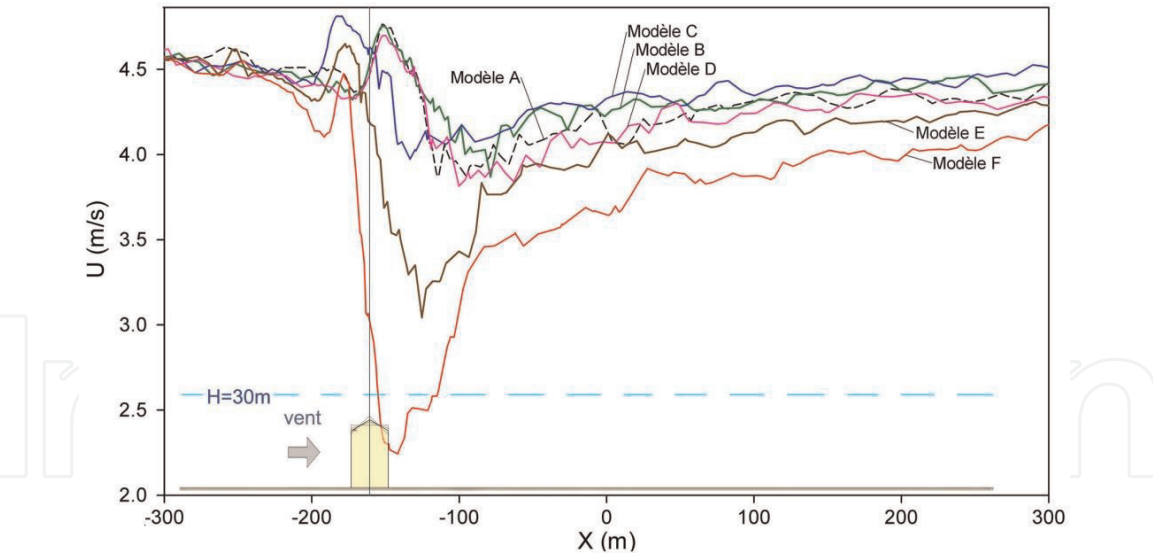
Figure 9.
Comparison of wind velocities on the central line in the wind direction at height H = 30 m (for gable roof models).
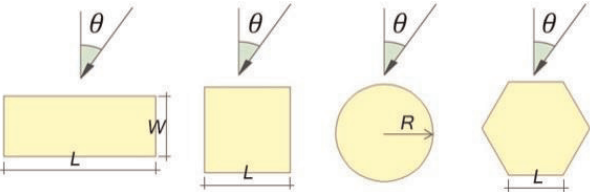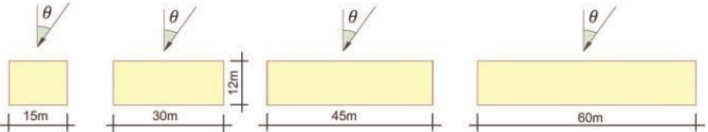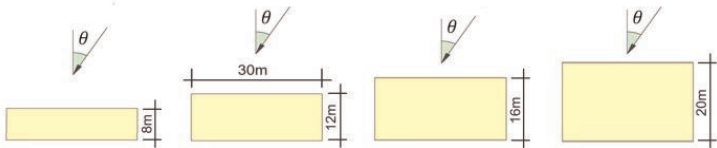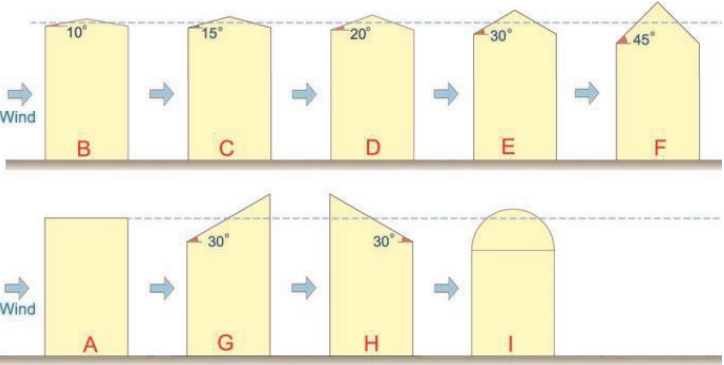

Figure 10.
Comparison of wind velocities on the central line in the wind direction at height H = 30 m (for different roof models).

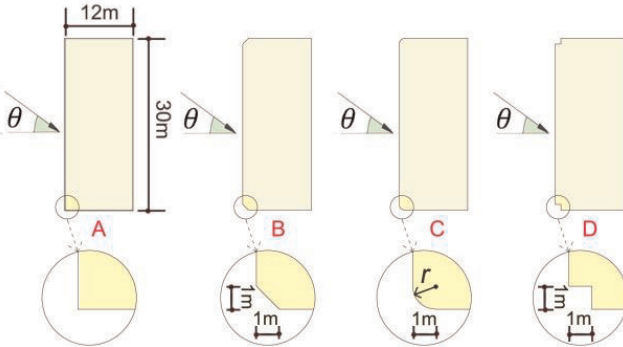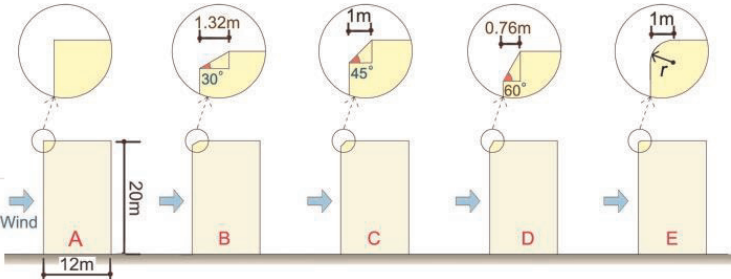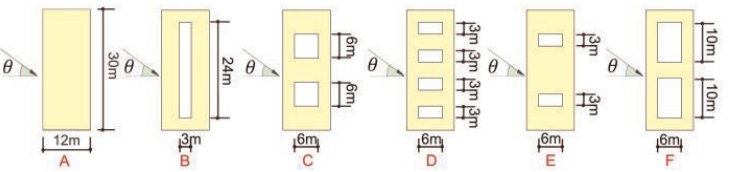(a = 10°), model D (a = 20°), model E (a = 30°), and model F (a = 45°). This order is exactly the same as that of assessing wind concentration above the roofs. The situations of the one-pitched roof models and dome model are also similar.
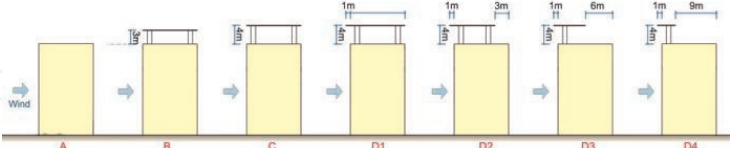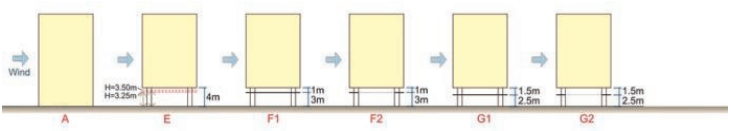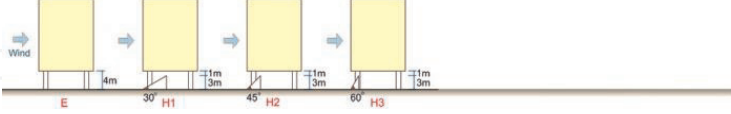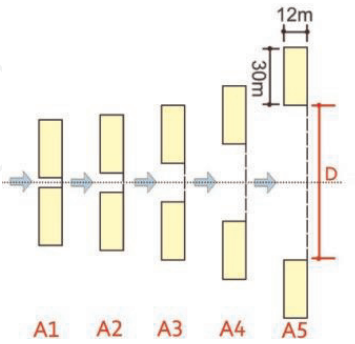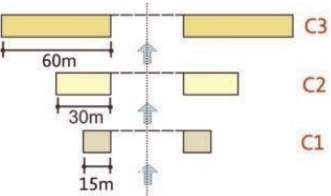
3.3 Wind evaluation with building forms parameters

In this chapter, indicator M is defined as assessing the total potential of wind energy on the surface, especially planes above the roof, because it is the most promising place to develop urban wind energy. Indicator D is defined as the wind energy density per surface unit. Indicator Cv is as well used as the wind velocity augmentation factor to evaluate the effect of wind concentration. Wind flow around some simplified geometric models is simulated and discussed.
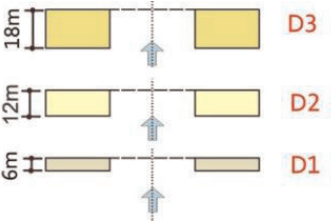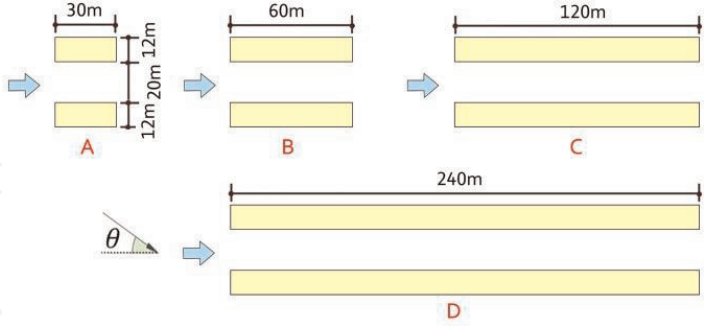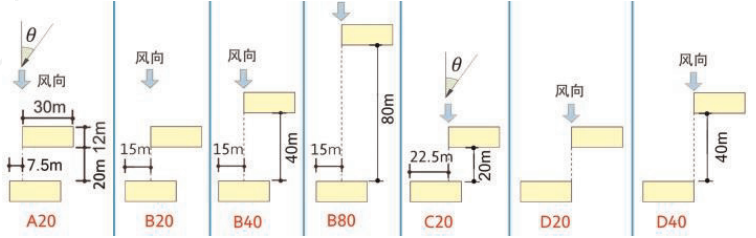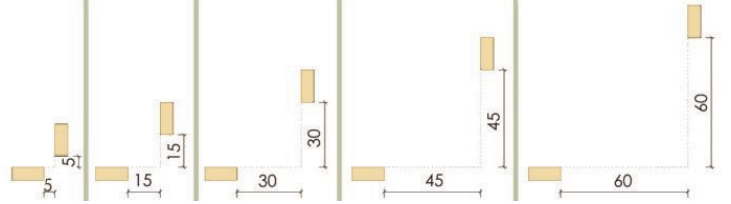
Actually, apart from the impact of building plane and roof shape, there are many other building form parameters that have much influence on wind potential. Different forms of 1–3 buildings are simulated and analyzed. Incidence angle and different evaluation height above the roof are considered. The following **Table 1**
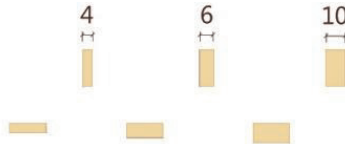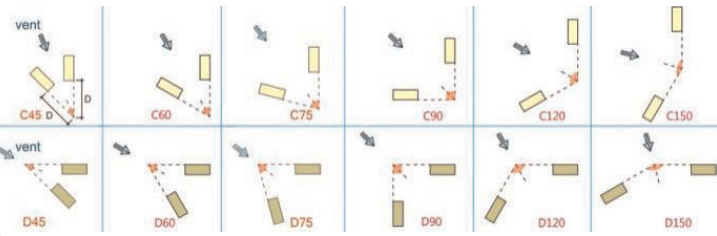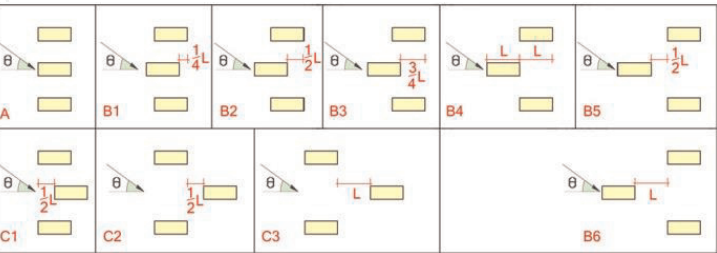
Parameters	Analyzed cases	Influence on the wind	Favor for wind potential development
Floor plan		Very big	Yes
Length		Big	Yes
Width		Small	No
Roof shape		Very big	Yes

12

Parameters		Analyzed cases	Influence on the wind	Favor for wind potential development
Corner	Exterior wall corner		Small	Yes
	Roof-wall corner		Very big	Yes
Courtyard			Small	No

Parameters		Analyzed cases	Influence on the wind	Favor for wind potential development
Wind passage	Roof canopy		Big	Yes
	Ground floor built on stilts with slab in between		Small	No
	Ground floor built on stilts with wedge		Big	No
Separation distance between two buildings			Small	No
Length of a pair of buildings facing wind			Big	Yes

Parameters		Analyzed cases	Influence on the wind	Favor for wind potential development
Width of a pair of buildings facing wind			Small	No
Length of a pair of buildings parallel to wind direction			Small	No
Stagger of two buildings			Big	Yes
Two buildings in perpendicular	Separation distance between the two		Big	Yes

Parameters		Analyzed cases	Influence on the wind	Favor for wind potential development
	Length of the buildings		Big	Yes
	Width of the buildings		Small	No
Position angles of the two building			Very big	Yes
Stagger of the two/three buildings			Big	Yes

Table 1.
Synthesis of morphological parameters of analyzed buildings and anticipation evaluation of their wind potential.

shows the general impact of different building forms on wind potential development.

For rectangular buildings with different lengths, we find that the value of wind potential density over roof *D* usually decreases with the increase of building length. So, buildings with lower lengths are windier over roof. However, the sum of exploitable energy must be taken into account. In fact, it counts both the wind speed and the exploitable area of wind potential. Sometimes, even if the wind is strong, buildings with lower lengths may have lower productivity in total.

With regard to the influence of the width of rectangular buildings, we have noticed that there is an optimum width for the maximum wind energy density above the roof. At an incident wind at an angle of 0°, the buildings with 30 m long and 20 m high have the best wind energy density when the width *W* = 12 m (compared with cases *W* = 8, 12, 16, and 20 m). The optimum width changes with wind incidence angles.

With regard to the influence of exterior wall corner shape (with a scale of 1/20 of building floor area) of selected buildings, the results of index *Cv* are as follows:

The truncated and concave models are usually better than those of rounded corners. In normal wind, the results of these two models are slightly better than those of the reference model without corner change; however, they are poor in the inclined wind (*θ* = 30°), especially at a low altitude above the roof.

The results for the corner shape of the roof edge show that all models with varying angles are windier on planes near the roof, compared to the reference model without any change, while at a high altitude, they are almost the same. Among different cutting corner models, the case with an angle of 30° shows a biggest average wind speed, which is similar to the round corner model.

With regard to the impact of courts on rectangular plan buildings, cases of various sizes and forms of the courts are being tested. The results of indicator *M* show that the models with courts are usually windier on the roof than those without courtyards. The maximum porosity model usually achieves the maximum wind potential over the roof. For the models with the same porosity, the influence of incident wind angle is significant.

As for the impact of wind passage, some wind passage models were tested. The results of index *Cv* show that the canopy on the roof accelerates the wind between the roof and the canopy (compared with the reference model without canopy), but slows down the wind above the canopy at the same altitude. The lower canopy model is windier underneath the canopy. A canopy with extension facing wind has a strong influence on the wind speed in the wind passage under the canopy. The shortening of the rear of the canopy also helps to enhance the wind concentration effect. The model with stilts and slab in between in the ground floor has better wind above the roof and between the slab and the ground floor ceiling, compared with the reference case. However, as the absolute wind velocity is low, the wind passage set for the ground floor is not suggested for wind potential development.

Regarding the effect of wind incidence angle, several models with different *W/L* (width to length ratio) and *H/L* (height to length ratio) are being tested. The results of *Cv* show that when the W/L ratio increases, the optimal incidence angle increases, while for square model, the optimal incidence angle is 45°. Similarly, when the building height (with same floor plan) rises, the optimum incidence angle of wind decreases.

With regard to the influence of wind behind buildings, different heights, lengths, and widths of buildings are evaluated. We found that the wind behind the building slows down with the height and length of the building, but gets stronger with the distance of the building. The width of building has little effect on the wind behind the building. At a low evaluation altitude (from the ground), i.e., *z < 1.25H*

(building height), the distance from the building rear D has the greatest influence on variation of wind velocity, followed by other parameters like H and L (building length). At a high altitude, i.e., $Z > 2.5H$, all the parameters L, W, and D have small impact on the wind behind building.

For the study of two buildings in one row, several models with different separation distances, heights, lengths, and widths are considered. Generally speaking, the coefficient Cv increases when the distance between two buildings increases up to a very large value. However, as the length and width of buildings increase, this wind concentration effect declines. Compared with the single building, the wind concentration effect over the roof of two buildings facing wind in one row requires a considerable evaluation height over roof.

With regard to the parallel study of two buildings, several street shape models of different lengths are being studied, and the Cv on the midline above the roof and in the street is studied. We find that wind above the buildings is generally slower than that of free wind at the same height. The downstream wind of a long street is stronger than that of a short one. The maximum Cv is obtained at a low altitude above the roof. However, wind speed usually increases with altitude, and wind concentration areas vary with the shape of buildings and evaluation altitude. Therefore, we can determine the optimal length of wind energy development above the roof. As for the results in streets of different heights, we find that the wind concentration effect is stronger in a short street near the downstream of the building, but in a long street, the concentration appears rather far away from the building rear in downstream.

For the study of two staggered buildings, several models with different separation distances are tested. The results of index Cv show that most models have larger wind around inlet angles −60 or −45°. At 60 or 45°, the wind potential is slightly smaller. The inlet angle of maximum wind concentration effect is about −60° at a low altitude and about −45° at a high altitude above the roof. The offset distance and incidence angle are very sensitive to the results. With the increase of separation distance between two buildings, the effect of wind concentration increases at the beginning, but decreases with separation distance, which means that there is an optimum distance between two staggered buildings to produce the maximum concentration effect at a certain angle of incidence.

In the study of two symmetrical buildings in perpendicular, several models are studied: different building sizes, different isolation distances, and different incident angles. The results show that the wind energy density above the roof increases at the beginning and then decreases with the separation distance between buildings. Compared with insulated buildings, two buildings in perpendicular can produce wind concentration effect in divergent modes for all models and in convergent mode for buildings with large separation distance. When the evaluation altitude rises, the best wind inlet direction is from 45 to 30 or 60°. Wind potential is more sensitive in convergent mode than in changing the separation distance between buildings. In convergent mode, it is better to have a long distance between buildings to have a higher wind potential over roof.

4. Urban form and wind energy

4.1 Urban form parameters for wind potential evaluation

For wind energy evaluation, among many urban form indicators, only those morphological indicators that have a close relationship with the wind flow are

Abbreviation	Urban form parameter	Description
BCR	Building coverage ratio	A parameter to describe the construction density. It is the ratio of building coverage area and the examined site area
PR	Plot ratio	A parameter to describe the construction density. It is the ratio of total construction area and the examined site area
$\overline{H}$	Average building height	The average height of all the buildings in discussion
σ_h	Standard deviation of the building heights	A parameter to describe the variation level of building heights in a site
$\overline{V_b}$	Mean building volume	A parameter to describe the dispersion level of the buildings with different heights. It is the ratio of total building volume and number of buildings counted
λ_c	Mean aspect ratio	It is the sum of building envelope including the surfaces of all the external walls and the roofs, divided by the site area
Ra	Absolute rugosity	A parameter to describe the roughness of a surface to resist the free wind. It is the average obstacle height over the whole examined area
Rr	Relative rugosity	Defined by the standard deviation of the building volumes
Po	Porosity	A ratio of the emptiness volume to the entire volume
Oc	Occlusivity	A parameter of the distribution of the built to un-built perimeter against height

Table 2.
Definition of selected urban form parameters for urban wind potential.

chosen, e.g., building coverage ratio (BCR) and plot ratio (PR), average building height, rugosity, porosity, etc. The definitions are given in **Table 2**.

4.2 Ideal urban form simulation

Before applying the urban morphological parameters on the real-world complex models, ideal urban form models with group of buildings in simple configuration can be tested, in order to reveal the impact of some single urban morphological parameter. Here, we will take the study of density as an example.

First of all, we set a combination of 24 identical buildings ($W \times L \times H = 12 \times 30 \times 20$ m) as the reference of ideal urban form. It is set in a hemisphere wind field with a radius of 400 m. The CFD software setting is generally the same with the case of isolated building, but some necessary changes are made, such as the size of domain and mesh precision, considering the recommendations of Best Practice Guide for wind flow simulation in the built environment. The disposition of the ideal urban form reference is symmetrical by the central line of domain in the wind direction. However, the distances between each row of buildings are set different deliberately, in order to generate some variation and enrich the results (**Figure 11**).

Based on the reference model, in order to evaluate the impact of density in a community scale, we set different building floor plan layouts for the 24 buildings. The variations of building width and length include: $W \times L = 12 \times 45$, 12×20, 18×30, 8×30, 12×10 m. These buildings however have the same height and central positions as the corresponding buildings in the reference model. In **Figure 12**, models B and C reflect the change of building length facing the wind, while models D and E reflect the change of building width. The building density (BCR) can be
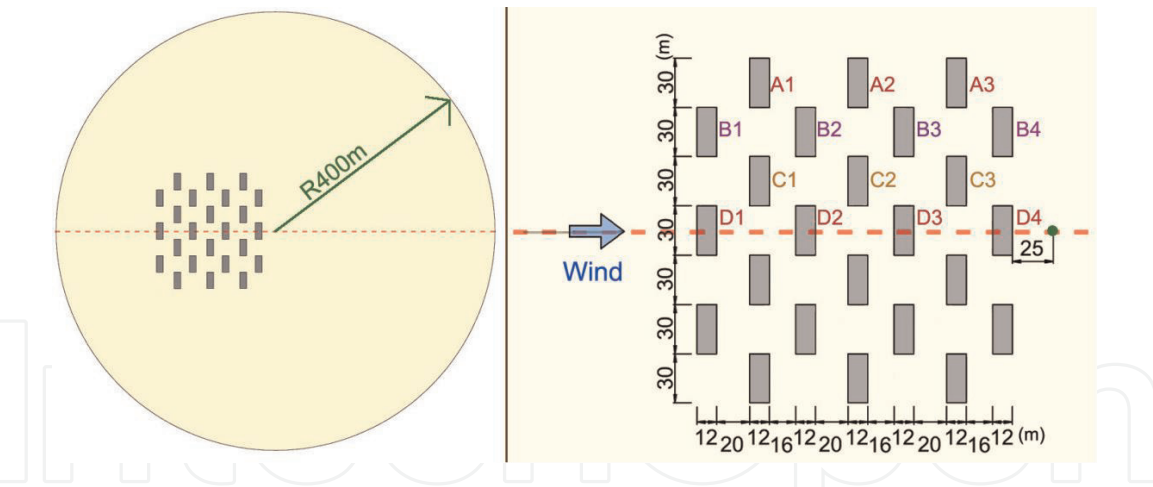
Figure 11.
Model of reference for analyzing the impact of density on wind potential (left: measure field layout and right: detailed disposition of buildings).
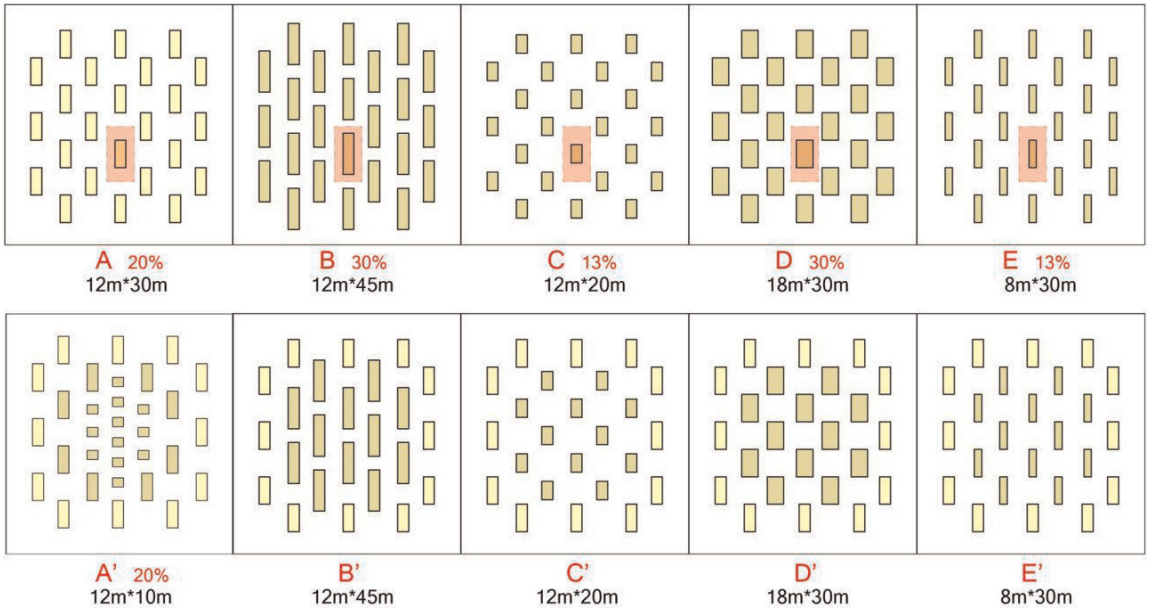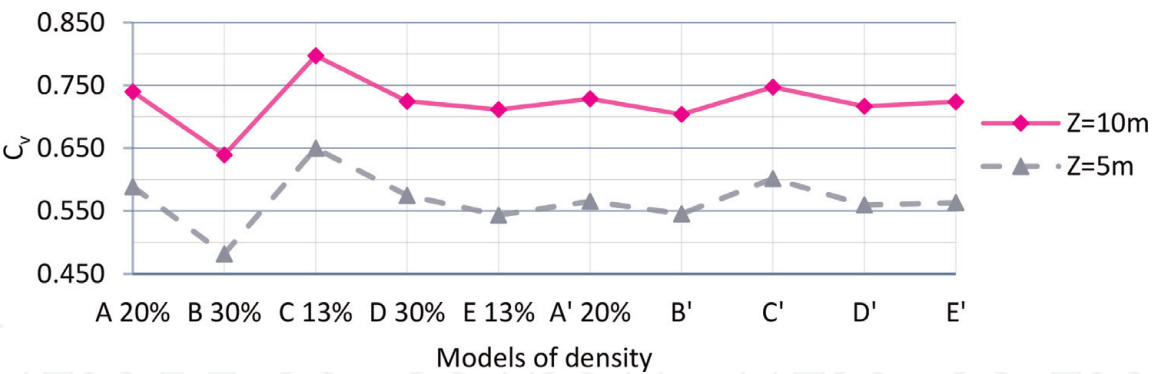

Figure 12.
Models for analyzing the impact of density by adopting different disposition of buildings.

calculate and varies among different models (A–E). In addition, in order to test and eliminate the impact of surrounding buildings, the "envelope" (most outskirt row of buildings) of the reference model is kept and the series of models B to E are changed to the series of B′ to E′. Apart from that, in order to evaluate the impact of fragmentation, the model A′ maintains the same density as the reference model A, but the four buildings in the center are divided each into three same fragments with the same distance between each other.

For the results of coefficient Cv of the wind potential above the roof (Z = 5 m and 10 m), the average values of all buildings in the center of each model are calculated to clearly understand the overall effect of density on the wind above the roof (**Figure 13**). The following conclusions can be drawn:

1. From the model A to model A′, the total wind potential above the roof decreases by 1.5–3.9%. That is to say, the fragmentation of building volume on floor plan with the same building coverage slows down the overall wind potential over roof.
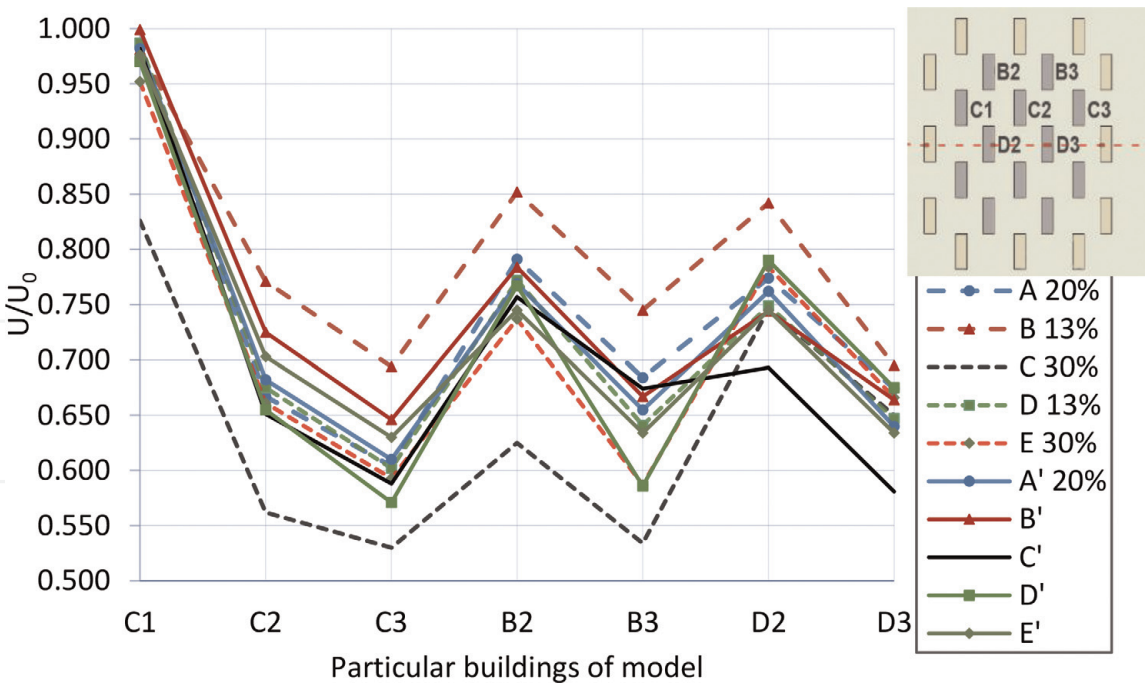
Figure 13.
Comparison of the average value of Cv for the model of density.

2. Among the models with buildings of different lengths (A, B, C, B′, and C′), the models (C and C′) with shorter buildings have larger wind over roof than other models. In addition, the energy efficiency above the central roof seems to be greatly affected by the surrounding area of the building, because the difference between models B and C is much greater than that between the models B′ and C′.

3. In the group of models with different building widths (A, D, and E), the difference of *Cv* values is very small. The decrease in building width (from D to A to E) is accompanied by an increase and subsequent decrease of *Cv* values. Therefore, there would be a most suitable width to maximize the wind effect.

4. In the group of models with the same density (B and D, or C and E), wind energy efficiency is different. It can be concluded that the influence of building length (face to wind) is far greater than that of building width.

In order to evaluate the influence of density in different areas of buildings in each model, we examined the *Cv* value over roof of each building (**Figures 14** and **15**). The values are averaged for those symmetrical buildings on both sides of the central line. The following conclusions can be drawn, with the decreasing order of *Cv* values of different buildings in the reference model A:
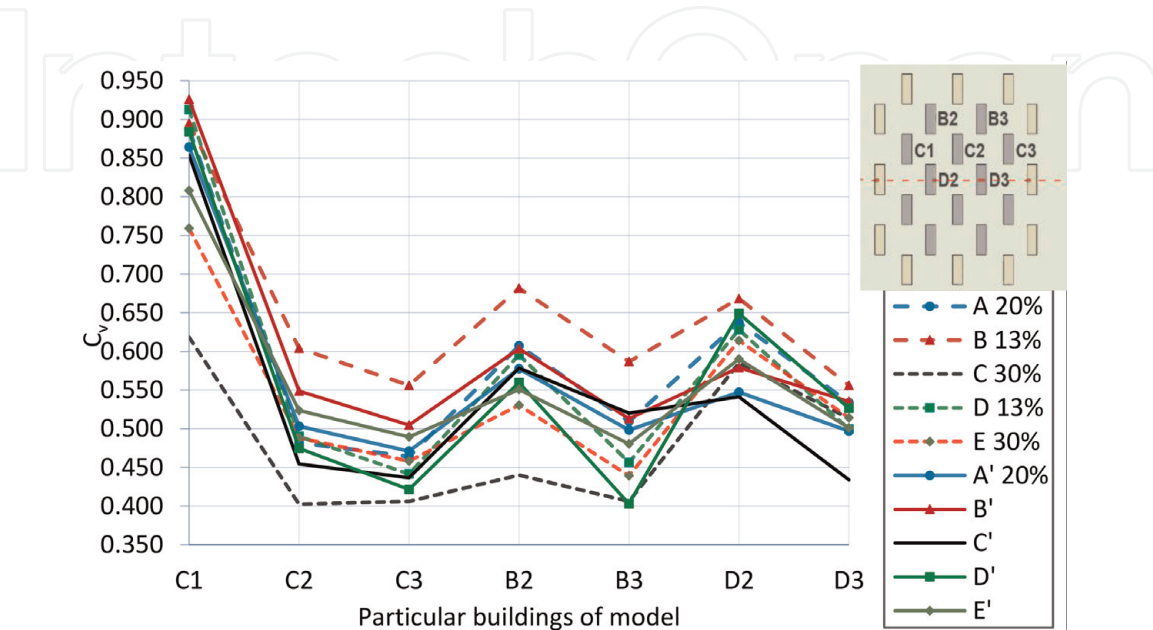
Figure 14.
Comparisons of Cv values of central buildings of different model of density (Z = 5 m).

Figure 15.
Comparisons of Cv values of central buildings of different model of density (Z = 10 m).

1. Usually, the buildings the more windward (e.g., B2, C1, and C2) have larger wind over roof than downstream buildings.

2. The buildings on the central line (D2 and D3) have Cv values relatively less affected by the shape changes of the buildings.

3. The fragmentation of building volumes (on plan) reduces the wind speed above the roof of most buildings, except for the building C2.

4. When the length of buildings changes (A, B, and C and A′, B′, and C′), the model with the lowest density has the highest wind speed above the roof of all buildings.

5. By reducing the building density around model B's central buildings, the wind speed over roof of most central buildings in model B′ is getting lower. In addition, with the increase of surrounding buildings' density, the wind speed of central buildings in model C′ is usually higher than that in model C (except for central-line buildings). Therefore, with the decrease of surrounding buildings' density, the wind energy efficiency over roof of central buildings decreases.

6. When changing the width of buildings (A, D, and E and A′, D′, and E′), the change trend of wind effect over roof is not clear.

4.3 Actual urban form comparison

As shown in the research structure in **Figure 2**, before selection of actual urban form for wind flow simulation, a primary filtration of urban forms need to be done in order to find out those who have high wind potential, based on empirical experience and evaluation. From the potential windy urban form group, six typical urban forms in six different cities in the world (Paris, Toulouse, Bombay, Barcelona,

Figure 16.
*Site plan of the six urban forms for comparison (extracted from Ref. [27]).*

New York, and Beijing) are selected. The scale of the central study area is 450 m × 450 m (red square in dash line), within an extended model representation of 350–450 m in radius. The site plans of them are shown in **Figure 16**. The color changes with the height of the building: the darker the color, the higher the height of the building. CFD simulation can evaluate wind energy by comparing different typical shapes according to different morphological characteristics. For comparison, the initial conditions are assumed to be the same, regardless of the local climate or socio-economic environment. Eight wind inlet directions with an interval of 45 are considered for every model. An average of wind potential over roof for the eight sessions is used for the comparison among them.

For the part of urban form study, the morphological indicator values of the six blocks show that the density of buildings varies greatly, ranging from 19 to 58% for building coverage ratio and from 1.1 to 12.1 for plot ratio; some blocks share similar PR (e.g., block of Toulouse and block of Bombay), but have very different building average volume and relative rugosity; some have very similar BCR and average occlusivity (e.g., block of Barcelona and block of New York), but with very different building average height, standard deviation of the building heights, mean aspect ratio, and absolute rugosity. With some similarities and differences, it is helpful to compare wind potential outcomes among these different urban forms. The detailed morphological parameter values can be found in Ref. [27].

For wind potential evaluation, three planes above the roofs (Z = 5, 10 and 15 m) of those highest buildings in study zone of each urban form is considered. They include all the potential buildings higher than the average building height of the study zone, as the previous experience and literature review show that evaluation height is a vital element that influences wind velocity. **Figure 17** shows the average values of coefficient Cv of wind over roofs of the highest groups of buildings (2–4 groups were given) of each model in every inlet direction scenario. And the minimum and maximum values, the total average change interval, and average range of the Cv values of each model were also summarized in **Table 3**.

With regard to the results of the velocity augmentation coefficient of different urban form models (**Figure 17** and **Table 3**), the following conclusions can be drawn:

1. Each model has its best inlet angle of wind to make use of the wind effect over roof of the highest building. For example, for the buildings of 24 m in block model of Paris, the wind from 15° is the strongest, and for the buildings of 50 m in block model of Toulouse, the strongest wind comes form −105°.

2. Compared with the free wind case (without buildings), there is little wind effect increase in blocks of Paris, Barcelona, and Beijing because of their *Cv* < 1, while the block models of Toulouse and Bombay has slight wind effect over roofs. The downtown block of New York has better situation, but the wind effect is limited to some of the tallest buildings in some inlet wind
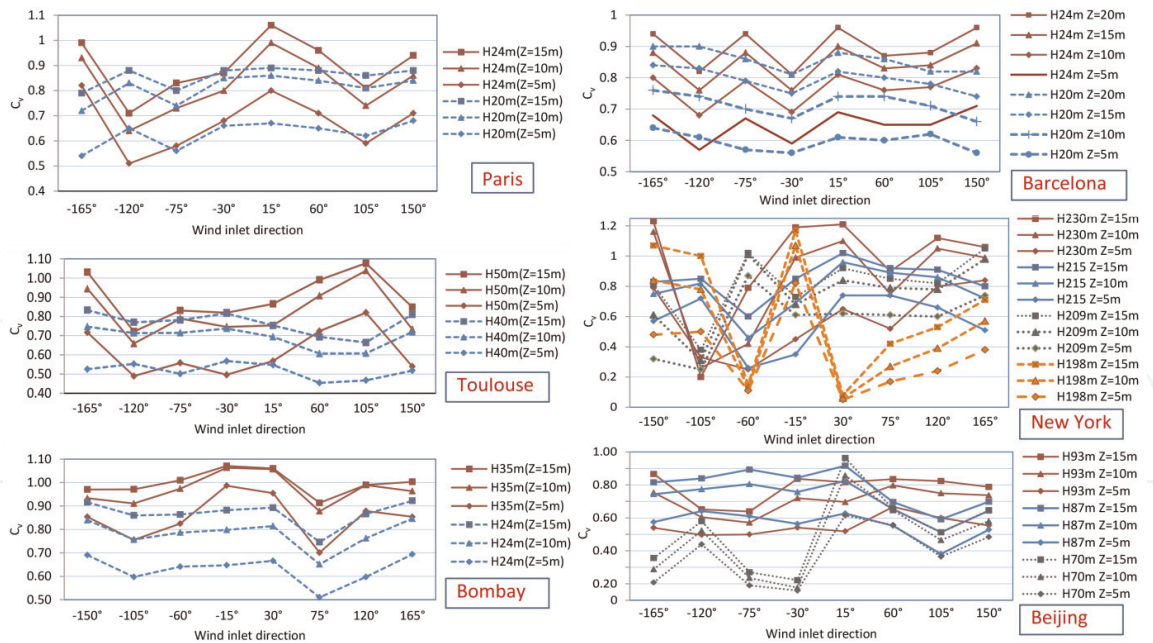
Figure 17.
Coefficient Cv of wind above the highest buildings of different urban forms.

	Paris	Toulouse	Bombay	Barcelona	New York	Beijing
Min	0.43	0.49	0.51	0.56	0.11	0.16
Max	1.06	1.08	1.07	0.91	1.23	0.96
Total average interval	0.63–0.86	0.54–0.80	0.67–0.90	0.61–0.81	0.50–0.80	0.54–0.76
Average range	0.228	0.259	0.221	0.193	0.300	0.219

Table 3.
Values of coefficient Cv of wind at different altitude over roof of the highest buildings in each model.

directions. One reason of the universal low wind effect may be the low level of evaluation. The Barcelona block model shows that the Cv value at $Z = 20$ m is higher than that at $Z = 15$ m above the roof (**Figure 17**).

3. With regard to the minimum and maximum values of Cv, it can be seen that the lowest values of the towers in block of New York and Beijing are quite astonishing, because they are less than 0.11 at $Z = 5$ m. The reasons may be the big roughness of the surroundings with many skyscrapers, and a tall building has a thicker turbulent layer above its roof than a lower building [36]. In addition, the highest Cv in block of New York is also the biggest among the six blocks. This is because the evaluated highest buildings are high enough (>200 m), which accelerates the wind around the building environment. However, with a lower height (<100 m), the highest buildings in Beijing block did not achieve a high Cv value. The reason may be that the heights of the tallest buildings in this model do not change much, which increases the wind turbulence around the near-roof areas.

4. In the total interval of Cv changes of each block model, it can be seen that the lowest, middle, and highest average values of the skyscrapers blocks (of New York and Beijing) are smaller than those of other blocks. In the range of Cv variation, we can see that most of the average ranges of Cv between $Z = 5$ m

and Z = 15 m are less than 0.3. *Cv* values of Toulouse and New York block models are more volatile than other blocks, i.e., both blocks have high level of turbulence than others. In fact, the coefficient values of variation of the building heights of these two models are also the largest among the six models.

Apart from the *Cv* evaluation, wind potential evaluation using the indicator of M′ is also undertaken. In **Table 4**, we can find the average values of the indicator *M′* at three altitudes over roofs, the average variation range of *M′*, heights of the highest buildings in each model, and total roof area of these buildings.

Based on the values in **Table 4**, the following conclusions can be drawn:

1. Blocks in Barcelona and New York have far more wind potential over roofs than other blocks. In fact, the two blocks have the largest roof area and can be used to develop wind energy. For New York block model, the reason may also come from its numerous high-rise buildings.

2. Comparisons between blocks in Paris and Barcelona show that most geomorphological indicators (BCR, PR, $\overline{H}$, λ_c, R_a, and P_o) of the two models change very little, and their great difference in wind energy potential between each may bear the reason of their big difference in building height variation. In other words, dramatic changes in the heights of buildings in model may increase wind energy over roofs. In fact, in comparing with blocks in Toulouse and Bombay, which also have similar building density, we have noticed that the block in Toulouse has higher wind energy potential and higher building height variation.

3. Block in Beijing has moderate wind energy potential. Although its average building height is very high (56.6 m), its total roof area is very small compared with blocks in Barcelona and New York. However, even block model of Beijing has less roof area than that of Paris, as its average building height is much higher than that of Paris, it has better greater potential.

In addition, considering the cut-in speed of wind turbines for useful power production, normally only wind with speed higher than 2 or 3 m/s (depending on the choice of wind turbine) can be taken as exploitable wind potential. Therefore, some refinement would be done to evaluate the exploitable wind potential of each urban form. The detailed results and analysis can be found in Ref. [27].

		Paris	Toulouse	Bombay	Barcelona	New York	Beijing
Average M′ value at Z = 15 m		1.74	1.46	0.79	3.50	3.82	2.03
Average M′ value at Z = 10 m		1.17	1.14	0.59	2.32	2.77	1.54
Average M′ value at Z = 5 m		0.57	0.49	0.32	1.70	1.23	0.72
Average variation range of M′		0.54	0.42	0.26	0.73	0.98	0.89
Highest buildings (H > $\overline{H}$)	Heights (m)	20, 24	27, 40, 50	24, 35	20, 24, 27, 32	87–230	70, 87, 93
	Total roof area (m²)	37,588	16,724	13,223	85,260	42,482	24,220

Table 4.
Results of M′ of the real urban form models for comparison (unit of M′ value: 10^6 m^5 s^{-3}).

4.4 Urban form unit simulation

In order to compare urban forms and make them applicable worldwide, here we adopt three simplified urban block models in Beijing (defined as Units 01, 02, and 03) and a simplified urban block model (defined as Unit 04) in Hong Kong. In addition, based on the model of Unit 01, the model of Unit 01b is created by removing a tower and implementing the buildings in order to make the model more or less symmetrically. Based on the model of Unit 04, the model of Unit 04b excludes its three corner buildings. Therefore, it is suggested that the impact of this change be tested for wind potential evaluation. The locations and sizes of the buildings in the four prototype units (Unit 01–04) are fully in line with the actual situation. Modifications to unit 01b and 04b are small and acceptable and "feasible" in sense of practice. We represent these unit models in actual conditions (building shape and location) to meet building requirements (e.g., for a plan of large housing tower) and urban planning requirements (e.g., in urban planning) as much as possible. Each model for unit study represents nine identical units, and the central unit is used as the research object. Unit sizes range from 170×170 to 430×330 m. The site plan and perspectives of the unit models can be seen in **Figure 18**.

Formally, Unit 01 and Unit 03 are a group of residential towers in form of pillar, Unit 02 is a group of residential towers in form of bar, and Unit 04 is a group of residential towers in form of pillar with chamfering. **Table 5** and **Figure 19** show the morphological values of each model, which is mostly the same as the corresponding real actual block model. At the same time, we can see that the building density of the four unit models in Beijing is similar.

As the previous actual urban form comparison models, urban form unit models adopt the same methods to evaluate wind effect and potential over roofs. An example of flow simulation in wind inlet direction of 60° at a horizontal plane of $z = 50$ m above the ground is given in **Figure 20**.

Table 6 lists the average and magnitude of Cv values for all wind inlet directions and three different evaluation heights over roofs. Their variation intervals at $Z = 10$ m and the favorable wind inlet directions for wind effect are also given.
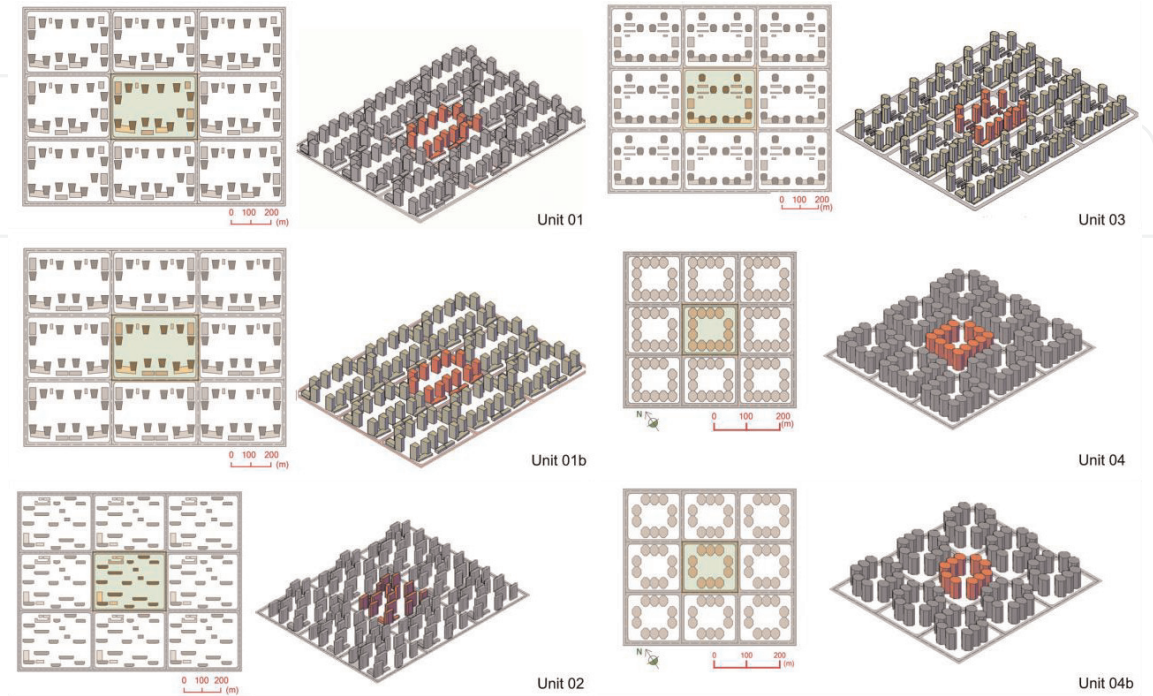
Figure 18.
Site plan and perspectives of the unit models.

| Morphological indicator	Site location					
	Jinsong, Beijing Unit 01	Jinsong, Beijing Unit 01b	Jinsong, Beijing Unit 02	Jinsong, Beijing Unit 03	Hung Hom, Hong Kong Unit 04	Hung Hom, Hong Kong Unit 04b
Type of urban form	Social apartment	Social apartment	Social apartment	Social apartment	Social apartment	Social apartment
Site area of the unit (m^2)	142,145	142,145	134,522	136,583	26,200	26,200
BCR (%)	19.09	19.42	14.12	19.13	35	26.92
PR	3.59	3.40	3.15	3.49	5.95	4.58
$\overline{H}$ (m)	59.53	55.50	70.01	57.53	50	50
Maximum height of building H_{max} (m)	87	87	87	93	50	50
$\sigma_h/\overline{H}$ (%)	59.6	65.1	44.4	72.1	0	0
$\overline{V_b}$ (m^3)	80,744	76,611	66,458	62,627	35,250	35,250
λ_c	1.46	1.39	1.60	1.36	2.48	2.63
R_a (m)	11.36	10.78	9.89	11	17.5	13.46
R_r (m^3)	46,053	46,933	39,613	55,563	0	0
P_o (%)	88.3	88.9	89.3	89.8	70.8	77.6
O_c (%)	57.24	55.71	60.17	55.28	63.31	58.14

Table 5.
Description of morphological parameter of urban unit model.
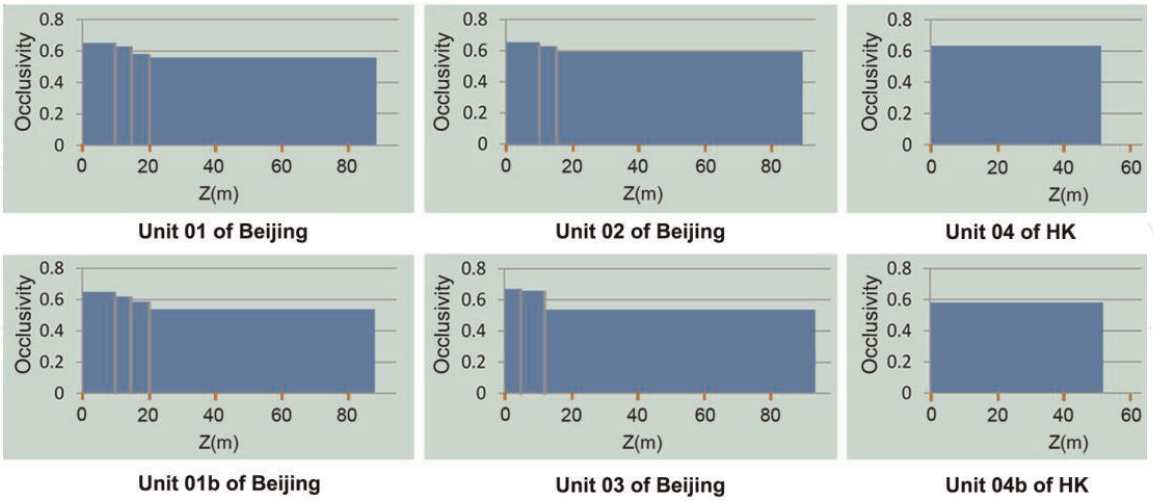
Figure 19.
Occlusivity values of the unit models.

Based on the results of **Table 6**, the following conclusions can be drawn:

1. Compared with the real block model in Beijing, the values of Cv of all these urban unit models with similar building structures are much lower. For example, at the height of Z = 15 m, the average Cv is equal to 0.87 over the roof of an 87 m tower in Beijing real block model, while in unit model cases (Units
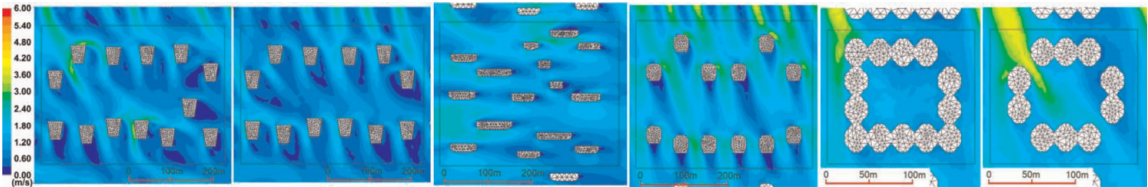
Figure 20.
Wind velocity contour lines of the unit models in 60°.

	Beijing Unit 01	Beijing Unit 01b	Beijing Unit 02	Beijing Unit 03	Hong Kong Unit 04	Hong Kong Unit 04b
Average value of Cv at Z = 15 m	0.49	0.51	0.50	0.56	0.39	0.44
Average value of Cv at Z = 10 m	0.43	0.46	0.45	0.51	0.34	0.38
Average value of Cv at Z = 5 m	0.35	0.37	0.37	0.39	0.26	0.30
Variation interval of Cv at Z = 10 m	0.36–0.54	0.38–0.56	0.25–0.64	0.45–0.57	0.20–0.43	0.32–0.46
Average variation range of Cv at Z = 10 m	0.178	0.184	0.375	0.113	0.216	0.142
Favorable wind inlet directions	−75, −120°	−75, −120°	−165, 15°	−75, 60°	60, −120°	−120, 60°

Table 6.
Results of Cv for the unit models.

01, 01b, and 02), it is around 0.50 for the tower with the same height. This may be because the roughness of the research area of the unit model is very large, because the other eight identical units are installed all around.

2. When the wind inlet direction changes, it can be found that the variation interval of *Cv* of the towers in form of bar element (Unit 02) is much larger than that of the towers in form of pillar (01, 03 element). This means that the urban form of buildings in form of bar is more susceptible to wind direction changes than the model of buildings in form of pillar.

3. For Unit 01 model, if a tower is removed and the space between towers is enlarged, then the new model (Unit 01b) has a general *Cv* slightly higher than the original one. The most advantageous wind inlet direction for wind effect does not change.

4. When comparing Units 01b and 03 of buildings in form of pillar with very similar morphological parameter values, we note that Unit 03 has a larger wind augmentation effect than Unit 01b. On the average variation range of *Cv* in different wind inlet direction, Unit 03 has a smaller value than Unit 01b. This probably because the studied towers of Unit 03 (93 m high) is higher than that of Unit 01b (87 m), and the form with chamfering has advantage on accumulating wind effect around the building.

5. For the case of Unit 04b which removed three corner towers from Unit 04, we note that the *Cv* of renewed Unit 04b is slightly higher than that of Unit 04.

	Beijing Unit 01	Beijing Unit 01b	Beijing Unit 02	Beijing Unit 03	HK Unit 04	HK Unit 04b
Average M' value at Z = 15 m	0.413	0.377	0.460	0.505	0.143	0.191
Average M' value at Z = 10 m	0.296	0.263	0.355	0.358	0.089	0.125
Average M' value at Z = 5 m	0.161	0.137	0.212	0.166	0.043	0.061
Average variation range of M'	0.279	0.246	0.613	0.205	0.124	0.116
Heights of towers (m)	87	87	87	93	50	50
Total roof area of the studied towers (m²)	16,939	15,636	14,608	15,072	9165	7050

Table 7.
Results of M' for the unit models (unit of M' value: 10^6 m^5 s^{-3}).

The average variation range of different wind inlet direction is becoming much lower. The most advantageous angle of wind inlet direction remains unchanged.

Based on the results in **Table 7**, the following conclusions can be drawn:

1. With a total area of the exploitable roof 8% less than that of Unit 01, Unit 01b has a total wind potential M' value 12% smaller than that of the original Unit 01 (averaging with results of three altitudes over roofs), although its *Cv* is slightly higher (around 5% on average).

2. Comparing the two similar models, Units 01b and 03 with buildings in form of pillar, it can be seen that the roof surface area of Unit 03 is 4% smaller than the other one; however, it has total wind potential with an average 30% higher. This may prove the advantage of the building form with chamfering on accumulating wind potential over roof.

3. The average *Cv* value of Unit 02 is slightly higher than that of Unit 01, and its total roof area is 14% smaller. The wind energy potential of Unit 02 is however 21% higher than that of Unit 01 on average. The reason may be that the high wind velocity variation can contribute much wind energy.

4. Compared with Unit 03, the total roof area of Unit 02 is reduced by 3% and its building density (BCR) is reduced by 10%. On the wind potential, Unit 02 has larger potential at a low altitude above the roof and Unit 03 has larger potential at a high altitude.

5. With total roof area 23% smaller than that of Unit 04, Unit 04b however has 28% higher total wind potential. It proves that, taking away the towers in three corners, if well considered, can increase much wind effect and wind potential over roof.

5. Application: Urban wind energy evaluation

In this section, an application of urban wind energy potential evaluation is given. Local conditions are considered in order to find a decent and practical solution for wind energy development.

5.1 Case study background

Jinsong block, chosen as the study case, is located with latitude 39°53′, longitude 116°28′, in the Chaoyang District and near the city center of Beijing. **Figure 21** shows its location in Beijing and some photographs of typical buildings in this block. Jinsong block was chosen because of these typical high-rise residential buildings, which have some uniformed shapes and whose heights are favorable for wind velocity accumulation. Apart from that, the environmental and climate pressure of Beijing, local developed socio-economical conditions and people's awareness of sustainable development, all together are beneficial for developing green energy like wind energy in this area.

For wind condition, the data of Chaoyang District is taken as reference. The Chaoyang District Meteorological Bureau provided the wind velocity distribution and wind rose of four seasons, based on the data from 1995 to 2002 (**Figures 21** and **22**). We can see that the Northwest wind is dominant. The average wind speed is 3.21 m/s in spring, 2.09 m/s in summer, 2.4 m/s in autumn, 2.98 m/s in winter, and 2.67 m/s in a year.

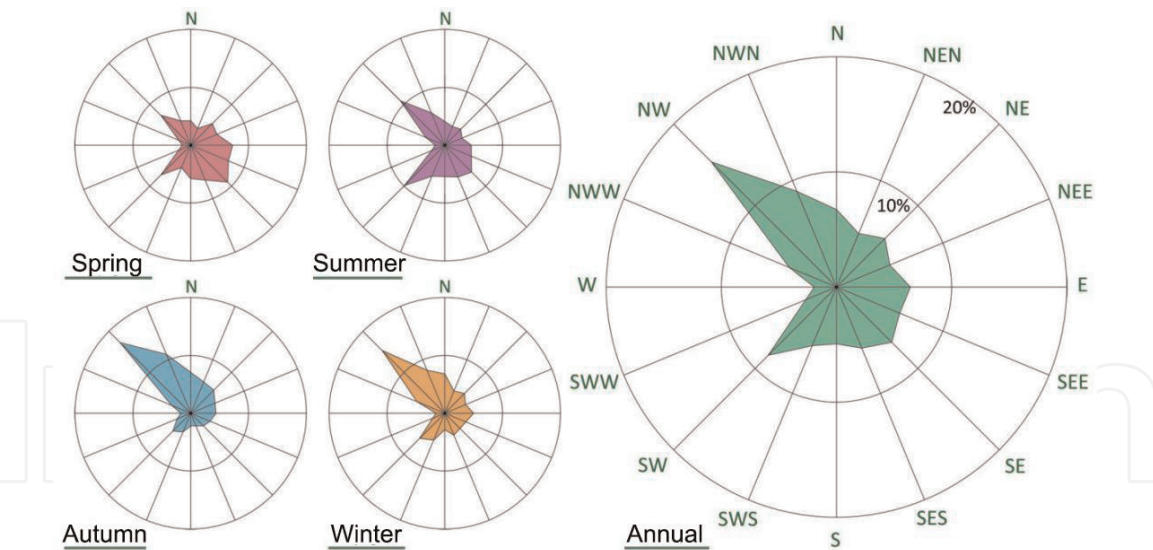## 5.2 Simulation model data and simplification

For the application case study, the model chosen has much bigger surrounding presentations than the real urban form comparison model. The study area in the center is 450 × 450 m and the presented surroundings zone has a size of 600 m in

Figure 21.
Position of the study area and the typical residential towers in it (source of pictures: map.baidu.com).
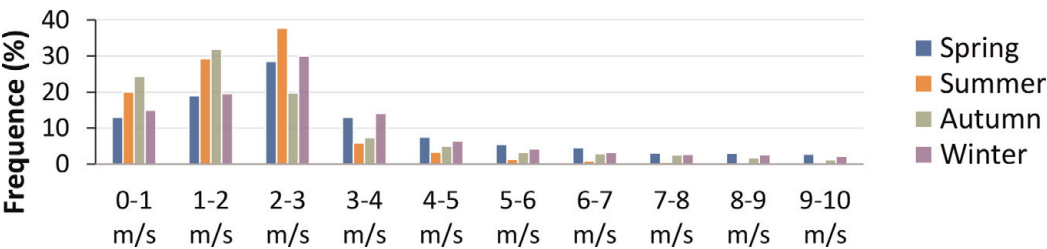
Figure 22.
Distribution of wind velocity of different season (source: Meteo Chaoyang).

Figure 23.
Simulation model before (up) and after (down) simplification.

radius. The domain size for simulation then is enlarged to a demi-sphere with a radius of 1200 m. CFD settings follow the previous experience and Best Practice Guidelines.

Considering running CFD simulation effectively and efficiently, model simplification and evaluation are necessary. For simplification, all buildings less than 10 m are neglected. Small volume buildings with the same height (which is also less than 24 m) are regarded as a connected entire block of the same height **Figure 23**.

Morphological information of the urban form of Jinsong block before and after simplification is shown in **Table 8**. Compared with the original model, the parameter values of the simplified model are roughly the same. Those parameters with a general big variation (>20%) are as follows: BCR, $\overline{H}$, σ_h, $\sigma_h/\overline{H}$, $\overline{V_b}$, and R_r. The plot ratio difference is only 3%. The influence of simplified model on wind energy assessment is analyzed. The results of wind potential M' values show that the impact

	Original model	Simplified model
Type of urban form	Social apartment	Social apartment
Study area (m^2)	202,500	202,500
BCR (%)	19.93	14.85
PR	3.57	3.47
$\overline{H}$ (m)	56.62	73.31
σ_h (m)	38.02	28.47
$\sigma_h/\overline{H}$ (%)	67	39
H_{max} (m)	93	93
$\overline{V_b}$ (m^3)	69,246	95,842
λ_c	1.41	1.35
R_a (m)	11.28	10.89
R_r (m^3)	50,130	34,429
P_o (%)	89.07	89.43
O_c (%)	57.60	58.38

Table 8.
Morphological information of the Jinsong block model before and after simplification.

of small buildings for this model is relatively small, averaging 4.75%. However, with simplification, the number of mesh of CFD model gets a relative huge savings: 24%. In this sense, the reasonable simplification can save much time for simulation and generally does not interfere the wind potential evaluation over roof.

5.3 Urban wind potential distribution analysis

As local wind rose, 16 wind inlet directions are considered for CFD simulation. In order to study the influence of urban form of Jinsong block on the wind potential, CFD simulation without local wind distributions is first undertaken and analyzed. **Figure 24** shows the average velocity augmentation factor (Cv) and total surface wind potential (M′) over roofs of the highest towers in the model. We can find that when the wind inlet directions are 112.5, 135, and −135°, the values of Cv and M′ are relatively smaller than in other wind inlet directions. That means, in these directions, the wind over roof is fable for this model.

Now considering the local wind roses (**Figure 25**), we can evaluate the actual wind potential over roof of the Jinsong block model (**Figure 26**). We note that 45° is the best wind inlet direction to develop the maximum wind potential.

In addition, in order to determine the location of wind turbines on the roof, the wind potential above each tower roof was evaluated (**Figure 27**). We found that the buildings C1, C2, D1, and E1 usually have the highest wind potential. The towers D3 and E2 have very big potential with an incident wind angle of 45°, but not very impressive with other angles. It is necessary to avoid choosing the towers C7, D4, D5, and D8, which actually have average or less wind potential over roof, regardless of the incident wind angle.

If we integrate the local wind distribution of wind rose over different inlet angles the CFD simulation results, then we can overlap the wind speed contour line maps (z = 80 m from ground) in different inlet angles with the corresponding percentage of transparency (**Figure 28a**). Then in order to evaluate wind potential around
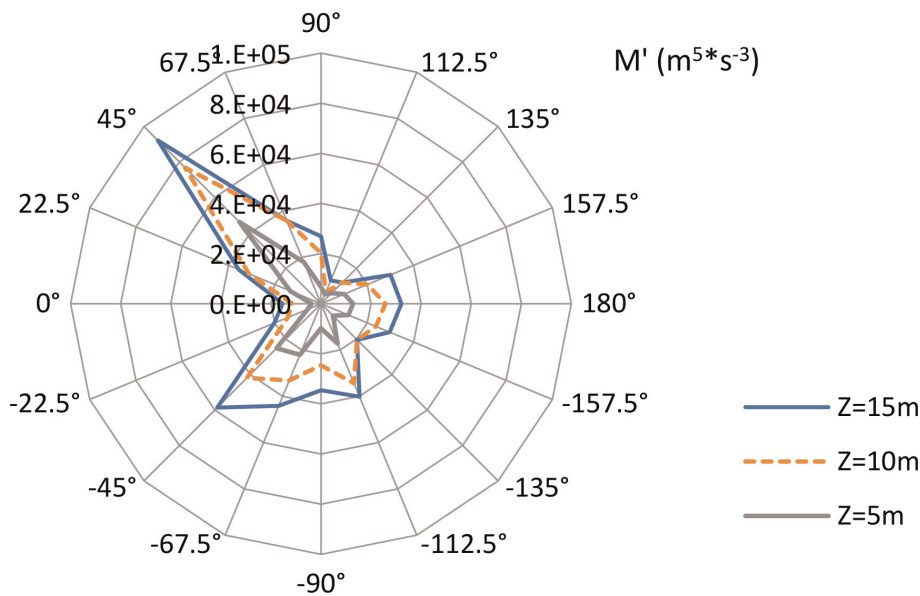

Original model

Simplified model
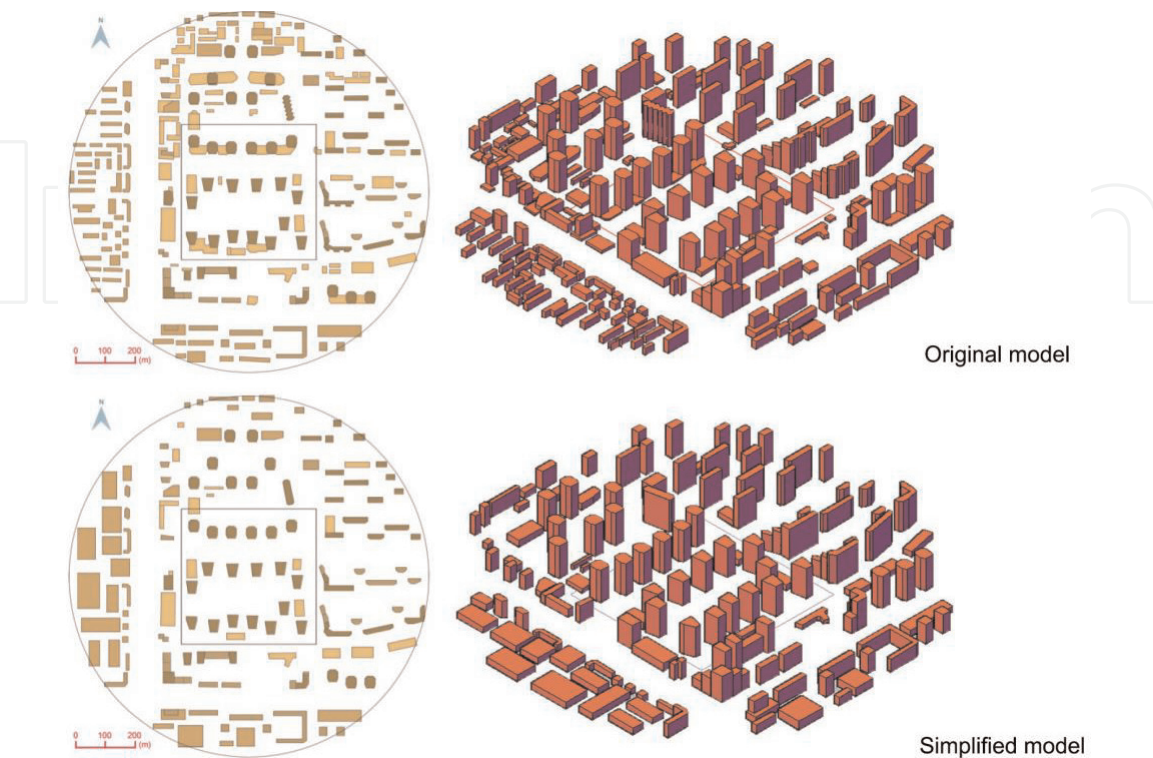
Figure 24.
Simulation results on distribution of Cv an M′ over different wind inlet direction (without local wind conditions).
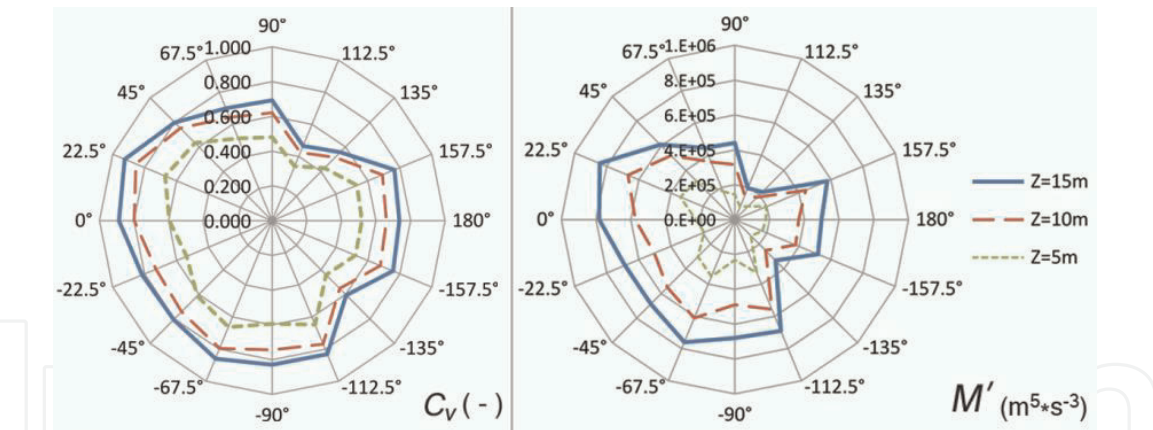
Figure 25.
Wind rose of Chaoyang District (source: Meteo Chaoyang).
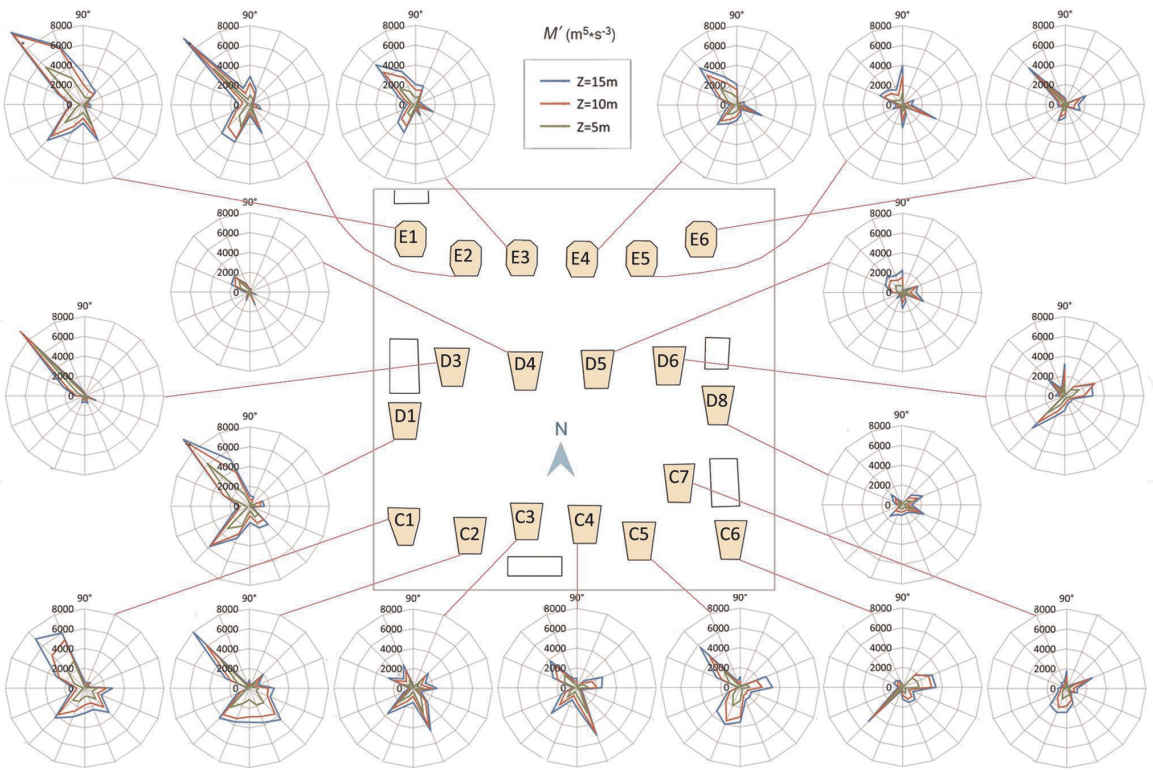

Figure 26.
Wind potential M' distribution with consideration of local wind conditions.

towers near the exterior walls (for vertical axis wind turbines), we made all the towers higher than 80 m having an offset dash line 5 m away from the external walls on plan. In order to better identify the area with the highest wind speed, the contour lines of wind speed bigger than 3.25 m/s is extracted and marked with yellow and red in **Figure 28b**. We find that the wind speed near the external walls is often very low. Only towers E1, E2, and E3 have "exploitable" wind potential near the external walls in some wind inlet angles. On the contrary, the wind above the tower D3 (70 m height) is much larger, although the tower D3 is not the best choice if we evaluate wind potential over roofs (**Figure 27**).

5.4 Urban wind installation and evaluation

Considering the relatively low speed and high turbulence intensity on the roof of Jinsong District, micro or small vertical axis wind turbines will be used. In fact, the average wind speed at $Z = 10$ m above roof is 2.3 m/s, and average wind turbulence intensity is 45%. Among many types of commercial wind turbines in the market, we found three types of wind turbines that can operate in low-speed wind: Beijio BDP-600/250, Archimedes Liam F1, and WindTronics BTPS 6500. The technical parameters of these turbines are shown in **Table 9**. After comparing several aspects
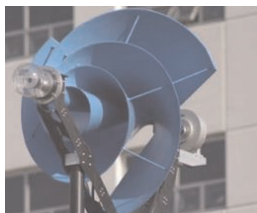
Figure 27.
*Wind potential M′ distribution over roof of different tower.*
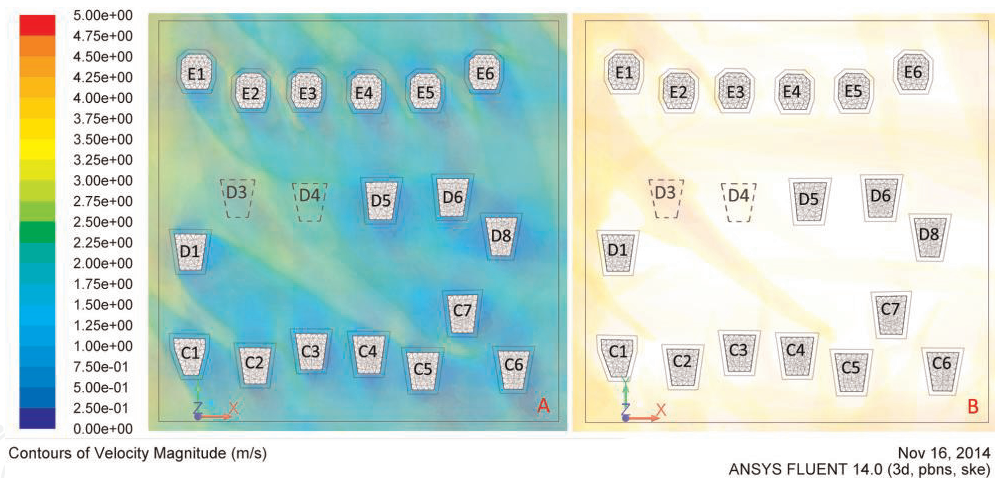
Figure 28.
Overlapping wind velocity profile (z = 80 m) of 16 inlet directions with consideration of local wind rose.
(A: profile with full level of velocity; B: profile with velocity bigger than 3.25 m/s).

including rated power and unit price, we decided to choose BDP-600/250 (Chinese Wind Turbine), which is actually workable in weak wind, light on weight, and the most economical among the three wind turbines. The power curve of the wind turbine is provided by the producer (**Figure 29**).

An example of installing wind turbine on the roof of tower E1 is introduced. Considering the size of the selected wind turbines and the space above the roof, we drew a wind turbine matrix to evaluate the wind power distribution of each wind turbines position. A distance of three rotor diameters between two wind turbines (axis to axis) in the direction perpendicular to the wind is considered. In the second row, the wind turbine is located in the middle of the interval between the two turbines in first row, and also three rotor diameters from each turbine. **Figure 30** shows the temporary arrangement matrix for wind turbines on the roof. According

		Beijio BDP-600/250	Archimedes Liam F1	WindTronics BTPS 6500
Rated power (W)		600	1000	1500
Rated wind speed (m/s)		8	12	14
Min. exploitable wind speed (m/s)		3	2	1
Size (W × L × D) (m × m × m)		1.8 × 1.8 × 1.4	1.5 × 1.9 × 1.75	2 × 2.2 × 0.5
Swept surface area (m^2)		2.5	1.8	2.5
Weight (kg)		42	75	110
Noise (dB)			<42	<35
Unit price ($)		1000	5450	5695
Power in experiment (W)	2 m/s	0	0	22
	3 m/s	48	10	58
	4 m/s	82	62	100
	5 m/s	130	141	163

Table 9.
Technical parameters of the selected wind turbines adaptive for fable and turbulent wind environment.
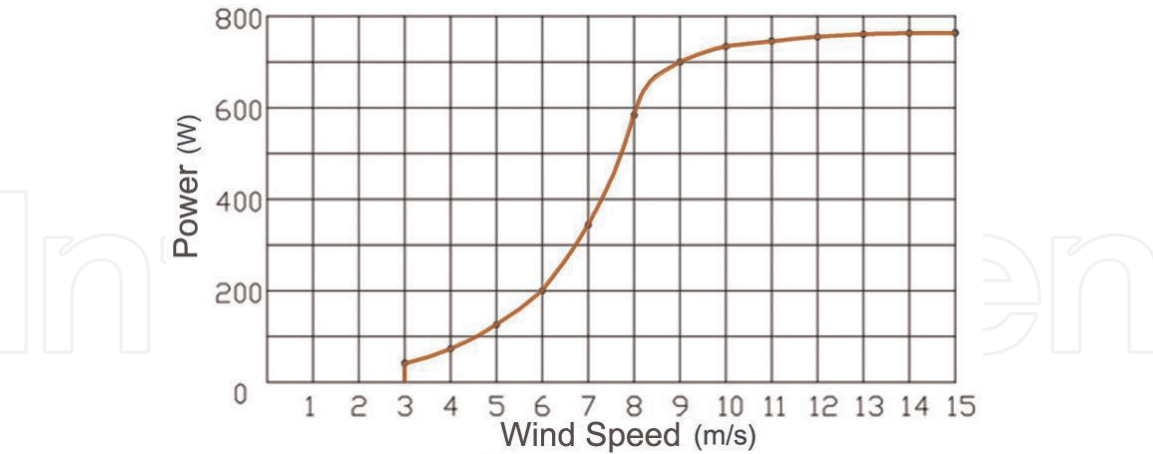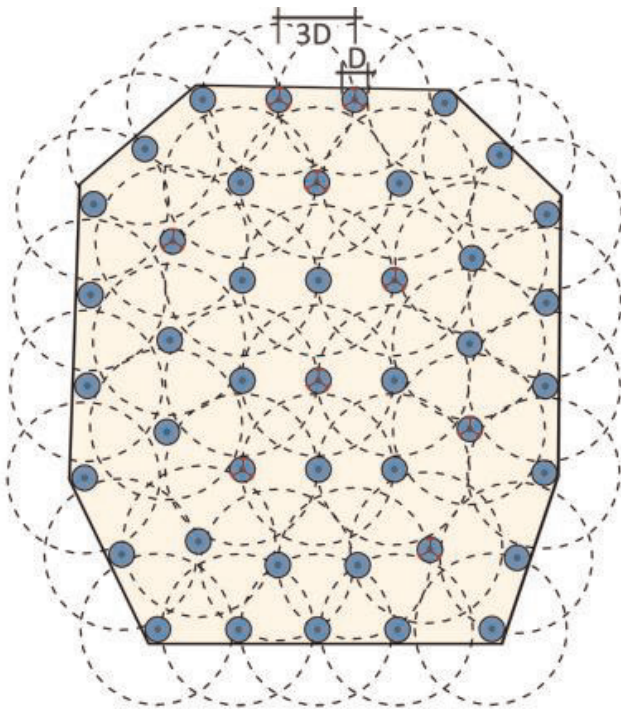

Figure 29.
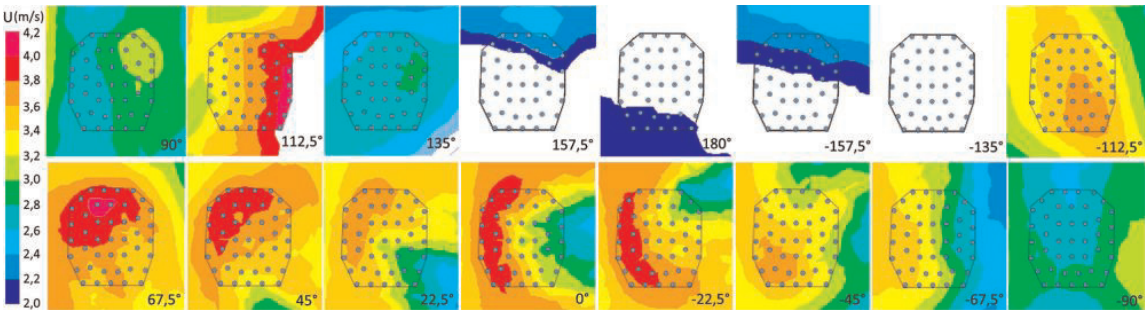*Power curve line of the wind turbine BDP-600/250 (source: detail.1688.com).*

to the research of Durrani and Qin [38], the T-shaped configuration of wind turbines mentioned here is conducive to enhancing the wind power generation of the second row turbine. Bayeul-Laine et al. [39] show that, in order to improve efficiency, the distance between two wind turbines in front row facing wind should be small, and the distance between two turbines in the direction of wind should be large. The ongoing arrangement of wind turbines would consider these suggestions.

In order to identify the wind potential of each installation location, the wind speed contour lines of 16 wind inlet directions at Z = 10 m above the roof of tower

Figure 30.
Potential positioning of wind turbines on the roof of the tower E1.

Figure 31.
Wind speed contour lines of wind at Z = 10 m over roof of the tower E1 in 16 wind inlet directions.

E1 are given (**Figure 31**). According to the power curve of wind turbine BDP-600/ 250, each wind speed value is calculated into a value of wind potential power. As we know that the wind power is a function of the cube of wind velocity, the local wind distribution data, rather than the average wind speed, are used to assess the potential of wind energy. Thus, the expected wind power generation capacity at each point can be calculated (**Figure 32**).

Figure 32 shows that the points with relatively strong wind potential lie on the edge of the northwest corner while this direction is the dominant wind of Chaoyang District. In fact, the average power of all these points is 91 W, and the difference between the points is not very large ($\pm$13 W). For example, if the windiest point (point 6, 103 W) is used, the payback period of the wind turbine installed here will be:

$$R_n = \frac{C_{turbine} + C_{support}}{R_{annual}} = \frac{1000 + 800}{0.103 * 24 * 365 * 0.1} = 20 \text{ yrs} \qquad (7)$$

where $C_{turbine}$ is the cost of wind turbine, $C_{support}$ is the supporting service cost that consists of masts, installation, civil engineering, and maintenance, and R_{annual} is equivalent to the annual income of electricity generation, 0.1 US dollar per kilowatt is the local electricity bill price.
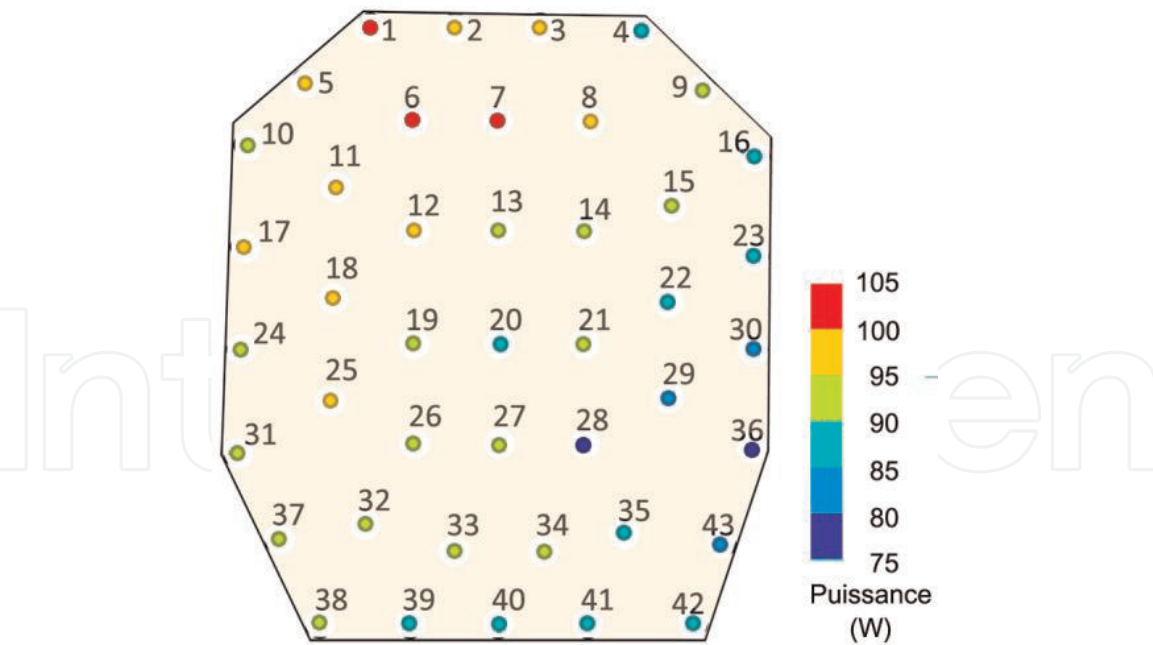
Figure 32.
Wind potential power of wind at Z = 10 m over roof of the tower E1.

Similarly, the payback period of the wind turbine at the lowest wind point on the roof of tower E1 (point 36) is found to be 26 years. Compared with other wind turbine economic analysis cases [37], as well as the aspects of policy subside and measures to improve wind effect over roof, the application of wind turbine BDP-600/250 on the roof of the windiest tower in Jinsong block is acceptable. However, given that tower E1 is one of the windiest locations in the block, we must recognize that the wind power potential over the roofs of other buildings in the block is relatively low and may hardly be "profitable."

6. Conclusions

This chapter shows a method to evaluate wind energy potential with urban morphology. Block scale (500 × 500 m) was adopted for typical urban form classification and selection. CFD method is used for wind flow simulation. CFD parameter settings were validated and evaluated with wind tunnel experiment. Methods of verification and Best Practice Guidelines were used for parameter adjust for different model.

Indicator *M* is defined to assess surficial wind potential on planes over roof. M′ is found to be an equivalent and effective alternative to it. Indicator *Cv* is used as the wind velocity augmentation factor to evaluate the effect of wind concentration. Because of the limits of the size and location of the exploitable wind zone adjacent to the exterior walls, it is not easy to explore and compare the wind potential near the walls. Wind potential over roof is generally stronger and more practical than that near the exterior walls to develop wind potential.

Simple building forms (1–3 buildings) were tested for exploring the impact of building form on wind potential. Some rules were found on the relationship between building form indicator and wind effect as well as wind potential over roof. These results provide a knowledge base for wind assessment in the built environment and provide a benchmark for the simulation study of the block models. Thirteen indicators were selected that might help to determine the impact of urban

morphology on wind. In particular, the parameter of density is analyzed with an ideal urban form model, in order to show the method to evaluate the impact of one single morphological parameter on wind potential over roof.

Real urban forms were then evaluated and compared in order to reveal the impact of different urban form parameter on wind potential. Six typical blocks in Paris, Toulouse, Mumbai, Barcelona, New York, and Beijing are modeled and compared. The results show that most block models have little wind effect over roofs of the highest buildings. Wind inlet direction is an important factor to influence wind effect and wind potential over roof of a model. The height of the building is the decisive factor to improve wind speed. Models with higher variation of building heights would have bigger wind effect and wind potential. The total area of the roof used to install wind turbines and the average height of the highest buildings in the model are among the most important factors for wind potential over roof of a model.

Urban form unit models are then considered to understand the impact of a certain urban form feature on wind potential. Six kinds of urban unit models were tested, based on some small modifications of the actual urban forms. The results show that the model with buildings in bars is sensitive with different wind inlet direction. At a small altitude above the roof ($Z < 10$ m), model with buildings in bars has bigger wind potential, while at a high altitude, it is the model with buildings in form of pillar that has better wind potential. Removing one or more buildings in one model can increase the average wind speed above the roof, but because of the loss of exploitable roof area, it may not ensure an increase in wind energy potential of the whole block. In order to develop wind energy on roofs, buildings with chamfering, truncated or rounded corners, is recommended.

Finally, a block model in Beijing is given for urban wind evaluation case study. With consideration of local wind distribution data, wind potential of Jinsong block model with 16 different wind inlet directions is evaluated. An example of most windy building in the block was chosen and wind velocity distribution on different point position on the roof is analyzed. With integrated consideration of scope of use, rated power, cut-in speed, and unit price of wind turbines, a Chinese wind turbine Beijio BDP-600/250 is proposed for the project. With turbine power curve data, the potential wind power of different position on the roof was calculated. With local market and electricity bill information, the payback period of the wind turbine on the selected tower is between 20 and 26 years. Therefore, the potential of wind power generation in Jinsong District is generally feasible, but the detailed assessment searching for the windy block and the windy tower is still essential.

This paper gives a general method to evaluate wind potential in built environment with building and urban form study. The work will contribute urban wind potential development and urban wind environment evaluation. For further research, parametrical study of typical urban forms indicator and corresponding wind energy potential evaluation is suggested.

Acknowledgements

Author details

Biao Wang
Department of Architecture, North China University of Technology, Beijing, China

*Address all correspondence to: bwang@ncut.edu.cn

IntechOpen

References

[1] Campbell N, Stankovic S, Graha M, Parkin P, van Duijvendijk M, Gruiter TD, et al. Wind energy for the built environment (project WEB), PF4.11. In: Procs. European Wind Energy Conference & Exhibition, Copenhagen, 2–6 July 2001. 2001. Available from: https://www.researchgate.net/publication/30416722

[2] Stankovic S, Campbell N, Harries A. Urban Wind Energy. London: Earthscan; 2009. DOI: 10.4324/9781849770262

[3] Dutton AG, Hqlliday JA, Blanch MJ, Energy Research Unit, CCLRC, The Feasibility of Building Mounted/Integrated Wind Turbines (BUWTs): Achieving their potential for carbon emission reductions. Final report, under contract of Carbon Trust (2002-07-028-1-6), 4 May 2005

[4] IT Power, Small wind turbines for the urban environment—State of the art, case studies & economic analysis. EIE/04/130/SO7.38591, Project WINEUR, 2005

[5] WINEUR, Wind energy integration in the urban environment. Deliverable 1.1, Technology inventory report. EIE/04/130/SO7.38591, Project WINEUR, 2005

[6] WINEUR, Aspects socio-économiques et acceptablité des éoliennes en milieu urbain—France. EIE/04/130/SO7.38591, project WINEUR, 2007

[7] Cace J, Horst E, Syngellakis K, Niel M, Clement P, Heppener R, Peirano E, Urban wind turbines—Guidelines for small wind turbines in the built environment. Project WINEUR; 2007

[8] Grignoux T, Gibert R, Neau P, Buthion C. Eoliennes en milieu urbain-Etat de l'art. Paris: ARENE Ile-de-France; 2006

[9] Yu WK. Current progress and future development of wind energy in Hong Kong [thesis]. Hong Kong: University of Hong Kong; 2011

[10] Turesson J. Potential for renewable energy sources (RES) in Grenoble, Delft [Master's thesis]. Stockholm: KTH Industrial Engineering and Management; 2011

[11] Shi S. The applied research of urban high-rise buildings wind energy and for designing of hybrid energy storage system [thesis]. Shijiazhuang: Hebei University of Science and Technology; 2011. in Chinese

[12] Zeng HS. Integration of renewable energy with urban design: Based on the examples of the solar photovoltaics and micro wind turbines [thesis]. Cambridge (Massachusetts): Massachusetts Institute of Technology; 2011

[13] Whaley DM. Low-cost small-scale wind power generation [thesis]. Adelaide: University of Adelaide; 2009

[14] Christianson M. Windmill power for City people: A documentation of the first urban wind energy system. Nasa Sti/recon Technical Report N; 1977

[15] Moreno D, Charreron D. Urban Wind Energy: Case Study Wind Turbine at LÄKEROL Arena. VDM Verlag; 2011. ISBN-13:978-3639366402

[16] Kalmikov A, Dupont G, Dykes K, Chan C. Wind power resource assessment in complex urban environments: MIT campus case-study using CFD analysis. In: AWEA 2010 WINDPOWER Conference. May 23-26, 2010. 2010

[17] Zhao H, Gao H, Li JW. Integrated architectural design with wind turbines in urban environment.

New Architecture (in Chinese). 2011;**03**: 45-48. DOI: 10.3969/j.issn.1000-3959. 2011.03.010

[18] Balduzzi F, Bianchini A, Carnevale EA, Ferrari L, Magnani L. Feasibility analysis of a Darrieus vertical-axis wind turbine installation in the rooftop of a building. Applied Energy. 2012;**97**:921-929. DOI: 10.1016/ j.apenergy.2011.12.008

[19] Stathopoulos T, Alrawashdeh H, Al-Quraan A, Blocken B, Dilimulati A, Paraschivoiu M, et al. Urban wind energy: Some views on potential and challenges. Journal of Wind Engineering and Industrial Aerodynamics. 2018;**179**: 146-157. DOI: 10.1016/j.jweia.2018. 05.018

[20] KC A, Whale J, Urmee T. Urban wind conditions and small wind turbines in the built environment: A review. Renewable Energy. 2019;**131**: 268-283. DOI: 10.1016/j. renene.2018.07.050

[21] Simoes T, Estanqueiro A. A new methodology for urban wind resource assessment. Renewable Energy. 2016; **89**:598-605. DOI: 10.1016/j. renene.2015.12.008

[22] Toja-Silva F, Kono T, Peralta C, Lopez-Garcia O, Chen J. A review of computational fluid dynamics (CFD) simulations of the wind flow around buildings for urban wind energy exploitation. Journal of Wind Engineering and Industrial Aerodynamics. 2018;**180**:66-87. DOI: 10.1016/j.jweia.2018.07.010

[23] Biao L, Cunyan J, Lu W, Weihua C, Jing L. A parametric study of the effect of building layout on wind flow over an urban area. Building and Environment. 2019;**160**:106160. DOI: 10.1016/j. buildenv.2019.106160

[24] Asfour OS. Prediction of wind environment in different grouping patterns of housing blocks. Energy and Buildings. 2010;**42**:2061-2069. DOI: 10.1016/j.enbuild.2010.06.015

[25] Liu S, Pan W, Zhao X, Zhang H, Cheng X, Long Z, et al. Influence of surrounding buildings on wind flow around a building predicted by CFD simulations. Building and Environment. 2018;**140**:1-10. DOI: 10.1016/j.buildenv. 2018.05.011

[26] Azizi MM, Javanmardi K. The effects of urban block forms on the patterns of wind and natural ventilation. Procedia Engineering. 2017;**180**: 541-549. DOI: 10.1016/j.proeng.2017. 04.213

[27] Wang B, Cot LD, Adolphe L, Geoffroy S, Sun S. Cross indicator analysis between wind energy potential and urban morphology. Renewable Energy. 2017;**113**:989-1006. DOI: 10.1016/j.renene.2017.06.057

[28] Biao WANG, Shuai SUN, Duan ML. Wind potential evaluation with urban morphology—A case study in Beijing. Energy Procedia. 2018;**153**:62-67. DOI: 10.1016/j.egypro.2018.10.078

[29] Hang J, Li YG, Sandberg M, Claesson L. Wind conditions and ventilation in high-rise long street models. Building and Environment. 2010;**45**(6):1353-1365. DOI: 10.1016/j. buildenv.2009.11.019

[30] Yuan C, Ng E. Building porosity for better urban ventilation in high-density cities: A computational parametric study. Building and Environment. 2012; **50**:176-189. DOI: 10.1016/j.buildenv. 2011.10.023

[31] Muehleisen RT, Patrizi S. A new parametric equation for the wind pressure coefficient for low-rise buildings. Energy and Buildings. 2013; **57**:245-249. DOI: 10.1016/j.enbuild. 2012.10.051

[32] Wang B, Cot LD, Adolphe L, Geoffroy S, Morchain J. Estimation of wind energy over roof of two perpendicular buildings. Energy and Buildings. 2015;**88**:57-67. DOI: 10.1016/j.enbuild.2014.11.072

[33] Wang B, Cot LD, Adolphe L, Geoffroy S. Estimation of wind energy of a building with canopy roof. Sustainable Cities and Society. 2017;**35**: 402-416. DOI: 10.1016/j.scs.2017.08.026

[34] Menter F, Hemstro B, Henrikkson M et al., CFD Best Practice Guidelines for CFD Code Validation for Reactor-Safety Applications, Report EVOLECORA-D01, Contract No. FIKS-CT-2001-00154; 2002

[35] Franke J, Hellsten A, Schlünzen H, Carissimo B. Best practice guideline for the CFD simulation of flows in the urban environment. COST 732: Quality Assurance and Improvement of Microscale Meteorological Models; 2007. Available from: http://refhub.else vier.com/S0167-6105(18)30227/sref98

[36] Lu L, Ip KY. Investigation on the feasibility and enhancement methods of wind power utilization in high-rise buildings of Hong Kong. Renewable and Sustainable Energy Reviews. 2009; **13**(2):450-461. DOI: 10.1016/j.rser.2007.11.013

[37] Debled A, Deblock J, Etude de faisabilité d'une implantation d'éolienne en milieu urbain à Roubaix et Templemars dans le cadre du projet européen WINEUR.IMPACT 2005/2006, Rapport d'activité. Grant agreement no. EIE/04/130/S07.38591. Project WINEUR; 2006

[38] Durrani N, Qin N. 2D Numerical analysis of a VAWT wind farm for different configurations. 49th AIAA Aerospace Sciences Meeting including the New Horizons Forum and Aerospace Exposition. Orlando, Florida; 4-7 January 2011. Available from: https://www.researchgate.net/publication/256463516

[39] Bayeul-Laine AC, Simonet S, Bois G. VAWT with controlled blades: Inuence of wake of one turbine on power coefficient on the next turbine. 5th IC-EpsMsO. Greece; Jul 2013:1-8. Available from: http://hdl.handle.net/10985/7254